Physics – Uspekhi **46** (2) 169 – 191 (2003)

REVIEWS OF TOPICAL PROBLEMS

PACS numbers: 11.10.Gh, **61.43.–j**, 64.60.Ak

Critical exponents of a three-dimensional weakly diluted quenched Ising model

R Folk, Yu Holovatch, T Yavors'kii

DOI: 10.1070/PU2003v046n02ABEH001077

Contents

Abstract. Universal and nonuniversal critical exponents of a three-dimensional Ising system with weak quenched disorder are discussed. Experimental, computational, and theoretical results are reviewed. Particular attention is given to field-theoretical renormalization-group results. Different renormalization schemes are considered with emphasis on the analysis of the divergent series obtained.

1. Introduction

This paper reviews properties of a three-dimensional weakly diluted quenched Ising model (Fig. 1)[1] in the vicinity of a critical point. If dilution by a nonmagnetic component is weak, i.e., a system is far from the percolation threshold, the magnetic second-order phase transition is maintained in RIM, though possessing novel features in comparison with the pure ($d = 3$) Ising model (see, for instance, review [1] as well as Ref. [2]). Static critical exponents of RIM have been the subject of detailed experimental [4 – 20], numerical [21 – 41], and theoretical [42 – 65] analysis for almost three decades.[2] Recently, new data were obtained both in experimental measurements [15 – 20] and in Monte Carlo simulations [33 – 40]. A theoretical breakthrough occurred over several months in 1999 – 2000 when the perturbation expansion series for RIM were extended from the 4th [54] through 5th [63, 64] to the sixth order [65, 66]. Therefore, a systematization of the large number of available results on the critical behavior of RIM seems to be timely and expedient.

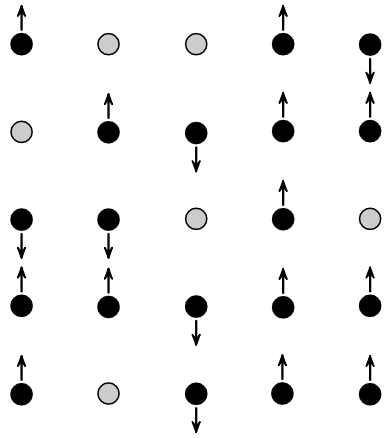

Figure 1. The weakly diluted quenched ($d = 3$) Ising model describes a system of scalar 'spins' randomly distributed and fixed in sites of a three-dimensional cubic lattice.

R Folk Institut für Theoretische Physik, Johannes Kepler Universität Linz, A-4040 Linz, Austria
Tel. (43-(0) 372) 24 68 83 99
E-mail: folk@tphys.uni-linz.ac.at
Yu Holovatch Institute for Condensed Matter Physics of the National Academy of Sciences of Ukraine, UA-79011, Lviv, Ukraine
Ivan Franko National University of Lviv, UA-79005, Lviv, Ukraine
Tel. (38-032) (2) 76 09 08
E-mail: hol@icmp.lviv.ua
T Yavors'kii Ivan Franko National University of Lviv, UA-79005, Lviv, Ukraine
Tel. (38-032) (2) 97 94 43
E-mail: tarasyk@ktf.franko.lviv.ua

Received 20 July 2001, revised 16 May 2002
Uspekhi Fizicheskikh Nauk **173** (2) 175 – 200 (2003)
Translated by T Yavors'kii; edited by S N Gorin

[1] We denote the random Ising model as RIM.

[2] Later in the review, only static critical behavior of RIM is considered. For recent Monte Carlo results of the dynamic critical behavior of RIM as well as their comparison with the theoretical data, see Ref. [3].

The subject of our discussion will be focused mainly on the RIM critical exponents. An *asymptotic critical exponent* x of a physical observable $\mathcal{O}(\tau)$ is defined [67] asymptotically close to the critical point T_c:

$$x \equiv -\lim_{\tau\to 0} \frac{\ln \mathcal{O}(\tau)}{\ln|\tau|} ,$$

where $\tau = (T - T_c)/T_c$ is the reduced distance to the critical point. For instance, the magnetic susceptibility χ diverges as

$$\chi \simeq \Gamma_{\pm}|\tau|^{-\gamma} , \quad \tau \to 0 , \tag{1}$$

where γ is the susceptibility critical exponent, while Γ_+ and Γ_- denote critical amplitudes above and below the critical point, respectively. The power law of type (1) holds exactly only in the asymptotic regime $\tau \to 0$. In this regime, the critical exponents and ratios of the critical amplitudes take constant values. According to the universality hypothesis, they are defined by global variables only. For a short-range interaction, the global variables are the space dimension and tensor characteristics of an order parameter. In the nonasymptotic regime, the approach to criticality is characterized by nonuniversal *effective critical exponents*, which are introduced to describe the behavior of a quantity in a certain temperature interval [68, 69]. The susceptibility effective critical exponent γ_{eff} by definition is written as:

$$\gamma_{\text{eff}}(\tau) = -\frac{\mathrm{d}\ln\chi(\tau)}{\mathrm{d}\ln\tau} . \tag{2}$$

In the asymptotic limit $\tau \to 0$, the effective and asymptotic exponents coincide. In the intermediate regime, the behavior is characterized by the so-called Wegner expansion [70]

$$\chi \simeq \Gamma_{\pm}|\tau|^{-\gamma}\left(1 + \Gamma_{1,\pm}|\tau|^{\omega\nu} + \Gamma_{2,\pm}|\tau|^{2\omega\nu} + \dots\right) , \tag{3}$$

where $\Gamma_{1,\pm}, \Gamma_{2,\pm}$ are nonuniversal amplitudes, ν is the correlation-length critical exponent, and ω is the correction-to-scaling exponent.

It is mainly the skill of the physicist which allows him or her to discriminate between regimes (1) – (3) either performing experimental measurements or doing theoretical calculations and numerical simulations. Below, we will review available data on effective and asymptotic critical exponents of RIM.

The paper is arranged as follows. In Section 2, we give general ideas about the influence of a weak quenched disorder on a second-order phase transition, formulate the model, and outline the main features of its critical behavior. Section 3 is dedicated to a survey of the experiments on weakly diluted uniaxial magnets. Data obtained by computer Monte Carlo simulations of RIM are considered in Section 4. In Sections 5 and 6, we outline the method of the renormalization group, which appeared to be the most fruitful theoretical tool in the study of the critical properties of RIM. We consider different renormalization schemes. Special attention is paid to analysis of divergent series, which reveal themselves as an intermediate step in the application of the method. In Conclusion, we discuss the main results and possible future directions of RIM studies.

2. Weakly diluted quenched Ising model

The central questions one has to answer in studying the influence of weak disorder on magnetic second-order phase transitions are (1) do the critical exponents of a homogeneous magnet change under dilution by a nonmagnetic component? and (2) if this is the case, are the new exponents universal? Regarding the first question, it has been argued [71] that if the heat-capacity critical exponent α of the pure system is positive, i.e., the heat capacity diverges at the critical point, then a quenched disorder causes changes in the critical exponents. This statement is known as the Harris criterion. Later, it was proven for a large class of d-dimensional disordered systems that the correlation-length critical exponent ν must satisfy the inequality $\nu \geqslant 2/d$ [72]. Both statements focus attention on studies of the $d = 3$ Ising model. In the case of the absence of structural disorder in this model, typical numerical values of the above exponents, together with the magnetic-susceptibility and the order-parameter critical exponents, were obtained by a resummation of the perturbation-theory series of the scalar $d = 3$ ϕ^4 theory [73]. They read

$$\alpha = 0.109 \pm 0.004 > 0 , \quad \nu = 0.6304 \pm 0.0013 < \frac{2}{3} ,$$
$$\gamma = 1.2396 \pm 0.0013 , \quad \beta = 0.3258 \pm 0.0014 . \tag{4}$$

According to the inequalities mentioned above, for the case of a diluted Ising model, new exponents are expected.

In order to obtain precise values of critical exponents, it is now standard to rely on renormalization-group methods. In particular, the theoretical estimates given in (4) were obtained on the basis of a deep analogy between the long-distance properties of the Ising model in the neighborhood of a second-order phase transition point and a field theory with an effective Landau – Ginzburg – Wilson Hamiltonian of the form

$$\mathcal{H}_{\text{Ising}}(\varphi) = \int \mathrm{d}^3R \left\{ \frac{1}{2}\left[|\nabla\varphi|^2 + m_0^2\varphi^2 \right] + \frac{\tilde{u}_0}{4!}\varphi^4 \right\} . \tag{5}$$

Here, m_0^2 is a bare mass squared, which is proportional to the distance to a critical point, and $\varphi = \varphi(R)$ and $\tilde{u}_0$ are the (bare) scalar field and coupling, respectively.

One of the ways to introduce quenched dilution to the effective Hamiltonian (5) is to add a random-temperature-like variable $\psi = \psi(R)$ [45] to m_0^2:

$$\mathcal{H}_{\psi}(\varphi) = \int \mathrm{d}^3R \left\{ \frac{1}{2}\left[|\nabla\varphi|^2 + (m_0^2 + \psi)\varphi^2 \right] + \frac{\tilde{u}_0}{4!}\varphi^4 \right\} . \tag{6}$$

One assumes that ψ obeys Gaussian distribution

$$P(\psi) = \frac{1}{\sqrt{2\pi w}} \exp\left(-\frac{\psi^2}{2w^2} \right) \tag{7}$$

with the dispersion w^2. Introducing n replicas [74] of model (5) in order to perform averaging over quenched disorder [75], one ends up [45] with a familiar effective Hamiltonian

$$\mathcal{H}_{\text{RIM}}(\varphi) = \int \mathrm{d}^3R \left\{ \frac{1}{2}\sum_{\alpha=1}^{n}\left[|\nabla\varphi_\alpha|^2 + m_0^2\varphi_\alpha^2 \right] + \frac{u_0}{4!}\sum_{\alpha=1}^{n}\varphi_\alpha^4 + \frac{v_0}{4!}\left(\sum_{\alpha=1}^{n}\varphi_\alpha^2 \right)^2 \right\} . \tag{8}$$

In the limit $n \to 0$, the field theory (8) describes critical properties of RIM. Here, the bare coupling u_0 is positive, being proportional to $\tilde{u}_0$, whereas the bare coupling v_0 is proportional to the minus variance of the random variable ψ

and thus is negative. The last term in (8) is present only for nonzero dilution (in the presence of disorder): it is directly responsible for the fluctuations' effective interaction due to the presence of impurities.

Often (e.g., in Monte Carlo simulations) the microscopic Hamiltonian of RIM is written in the following form:

$$H = -\frac{1}{2}\sum_{\mathbf{R},\mathbf{R}'} J\big(|\mathbf{R}-\mathbf{R}'|\big)\, S_{\mathbf{R}} S'_{\mathbf{R}}\, c_{\mathbf{R}} c_{\mathbf{R}'}, \tag{9}$$

where $\mathbf{R}$ runs over sites of a simple cubic lattice, J is the short-range translationally invariant interaction between pairs of $S = \pm 1$ 'classical' Ising spins, and $c_{\mathbf{R}}$ is the occupation number equal either to 0 or to 1. It is considered that geometrically the vacancies ($c_{\mathbf{R}} = 0$) are distributed independently according to the law

$$P(c_{\mathbf{R}}) = (1-p)\,\delta(c_{\mathbf{R}}) + p\delta(1-c_{\mathbf{R}}) \tag{10}$$

and fixed in different sites of the lattice (see Fig. 1). In (10), $p \leqslant 1$ is the concentration of occupied sites. Calculating free energy of model (9) and using a replica trick [74] to perform the configurational averaging of the logarithm of the configuration-dependent partition function, it can straightforwardly be shown that one ends up with the effective Hamiltonian of type (8) in the replica limit ($n \to 0$) with $u_0 \sim p$ and $v_0 \sim p\,(p-1)$.

From the viewpoint of dynamics, one can point to two opposite types of disorder. If a characteristic time of impurity dynamics is comparable to relaxation times in the pure system, impurity variables are treated identically to the 'pure' dynamical variables, since they are part of the phase space of the disordered system. The corresponding annealed disorder [75] is the subject of special investigations. Their main result states that the presence of annealed disorder leads to trivial consequences in the critical region. The so-called Fisher renormalization [76] states the following: if the heat-capacity critical exponent of an undiluted system α_{pure} is positive, then the critical exponents x of an annealed system are determined by those of the corresponding pure one (x_{pure}) by a simple renormalization in the form

$$x = \frac{x_{\text{pure}}}{1-\alpha_{\text{pure}}}\,, \quad \alpha = \frac{-\alpha_{\text{pure}}}{1-\alpha_{\text{pure}}}\,. \tag{11}$$

This explains why prevailing interest is attracted by the quenched disorder, when impurities can be considered as fixed and thus one needs to perform configurational averaging over an ensemble of disordered systems with different realizations of the disorder.

The Hamiltonian (8) represents critical properties of the problem (9) for small randomness. Alternatively, the scale-invariant fractal ramified cluster at the percolation threshold is a starting point of the strong-disorder approach. Here, the field-theoretic description starts with the effective Hamiltonian of the Potts model. A unified theory of the critical behavior of random systems, which would give regimes of both strong and weak disorder as its limiting cases, is still absent.

The translationally invariant Hamiltonian (8) presumes a perturbative account of thermal fluctuations around a spatially homogeneous unique ground state. Such an approach can be justified for pure systems. For random systems, in the region dominated by disorder there exists a macroscopic number of spatially inhomogeneous ground states. These correspond to local-minimum solutions of a saddle-point equation for the effective Hamiltonian (8) [77, 78]. Physically, this equation corresponds to the so-called Griffiths phase [79] caused by the existence of ferromagnetically ordered 'islands' in the temperature interval between the critical temperatures of pure and random systems. The description of the phase at the critical point is provided by a Hamiltonian with broken replica symmetry [77] and non-trivial properties [80, 81]. However, recently a refined analysis of the problem brought about a stability of the critical behavior of the weakly disordered systems with respect to replica-symmetry-breaking effects [82]. The theoretical results reviewed in the present discussion will be based on the replica-symmetrical Hamiltonian (8) (see Section 5).

The effective Hamiltonians (6) and (8) possess different global variables: although the space dimension is the same ($d = 3$), the symmetry and the number of the order-parameter components differ. Thus, one may expect that by application of renormalization-group approach they will lead to different models of critical behavior. One of the central notions of renormalization-group formalism applied to critical phenomena is that of the fixed point of the renormalization-group transformation. If a fixed point exists and can be reached from the initial values of the couplings, it corresponds to a critical point of the system. Applying the renormalization-group transformation to the effective Hamiltonian (6) and starting from positive values of u, one reaches the stable fixed point u^* which corresponds to the critical point of a $d = 3$ pure Ising model. The calculations in this case lead in particular to the results (4). The fixed point structure for the effective Hamiltonian (8) is sketched in Fig. 2. The earliest qualitative results about the structure of RIM fixed points appeared in the mid-seventies [43–45]. Later analysis supported this picture [48, 50]. Indeed, the fixed point I of the $d = 3$ pure Ising model appears to be unstable, and a new stable fixed point R appears (see Fig. 2). Thus, the general answer on the basis of the renormalization-group analysis of RIM supports the nonperturbative results of Refs [71, 72]: RIM critical behavior is governed by critical exponents different from those of the pure Ising model.

In the subsequent sections we will consider in detail how this statement was made clear in experimental, Monte Carlo, and theoretical studies.

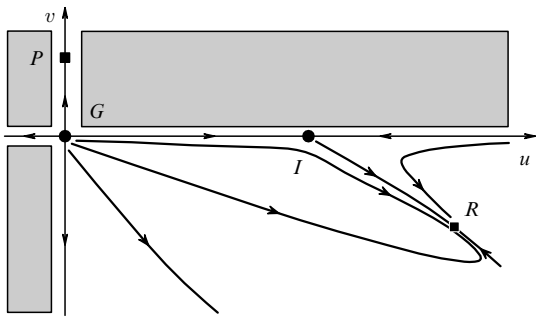

Figure 2. A qualitative structure of RIM fixed points. The Gaussian fixed point G is stable for $d \geqslant 4$, and the stable fixed point P cannot be reached from the initial coupling values $u > 0$, $v < 0$ (this region as well as other unphysical regions of RIM are shown in grey). The fixed point I of a pure Ising model is unstable. The fixed point R is both stable and accessible (stable fixed points are shown by squares).

3. Experimental study

In experiments on magnets, the Ising model is represented by crystals of difluoride of a transition metal, normally iron or manganese. In FeF_2, which possesses a rutile (tetragonal) crystal structure with lattice parameters $a = 4.697$ Å and $c = 3.309$ Å at room temperature [83], the spins of metal ions are ordered along the c axis in such a way that the spins of the body-centered ions are oriented in opposite directions to those of the corner ions. The system can be well described by a Heisenberg-like spin $S = 2$ Hamiltonian with a quadratic anisotropic single-ion term. It follows from the spin-wave dispersion relations on the basis of neutron scattering measurements [84] that other interactions constitute less than 6% of the interspin exchange force constant $J = 0.45$ meV. Dominant intersublattice exchange interaction and high anisotropy makes FeF_2 a very good experimental realization of an Ising antiferromagnet, where the order parameter is the sublattice magnetization. Experimental studies confirm that this substance possesses the pure Ising model critical behavior within the reduced temperature range $|\tau| < 10^{-1}$ ($\tau \equiv (T - T_N)/T_N$) around Néel temperature T_N. Another example is MnF_2 with similar crystal structure but with much weaker single-ion anisotropy in comparison with FeF_2. Nonetheless, the experimental study shows that this substance also belongs to the Ising universality class [85–87].

A material which corresponds to RIM can be obtained as a crystalline mixture of two compounds on the basis of a 'pure' Ising model matrix (see Table 1). A corresponding site-diluted uniaxial alloy is prepared by a substitution of

Table 1. The experimentally measured critical exponents of materials, which correspond to the random Ising model. *

References	Material	Method	$\lvert\tau\rvert$	β	γ	ν	α
Dunlap et al., 1981 [4]	$Mn_pZn_{1-p}F_2$ $p = 0.864$	NMR	10^{-3}	0.349 ± 0.008			
Birgeneau et al., 1983 [5]	$Fe_pZn_{1-p}F_2$ $p = 0.6; 0.5$	NS; LB	$10^{-1} - 2 \times 10^{-3}$ $2 \times 10^{-2} - 2 \times 10^{-3}$		1.44 ± 0.06	0.73 ± 0.03	-0.09 ± 0.03
Hastings et al., 1985 [6]	$Dy_3Al_5O_{12}$ +1% powder Y	MS	4×10^{-2}	0.350 ± 0.01		0.73	
Belanger et al., 1986 [7]	$Fe_pZn_{1-p}F_2$ $p = 0.46$	NS	$10^{-1} - 1.5 \times 10^{-3}$		1.31 ± 0.03	0.69 ± 0.01	
Barret, 1986 [8]	$Fe_pZn_{1-p}F_2$ $p = 0.9925 - 0.95$	NS	$10^{-1} - 10^{-3}$	0.36 ± 0.01			
Mitchell et al., 1986 [9]	$Mn_pZn_{1-p}F_2$ $p = 0.75$ $p = 0.5$ $p = 0.5$	NS	$2 \times 10^{-1} - 4 \times 10^{-4}$ $1 \times 10^{-1} - 5 \times 10^{-3}$, $\tau > 0$ $1 \times 10^{-1} - 5 \times 10^{-3}$, $\tau < 0$		1.364 ± 0.076 1.57 ± 0.16 1.56 ± 0.16	0.715 ± 0.035 0.75 ± 0.05 0.76 ± 0.08	
Thurston et al., 1988 [10]	$Mn_pZn_{1-p}F_2$ $p = 0.5$	SMXS	$6 \times 10^{-2} - 1 \times 10^{-3}$	0.33 ± 0.02			
Rosov et al., 1988 [11]	$Fe_pZn_{1-p}F_2$ $p = 0.9$	MS	$1 \times 10^{-1} - 3 \times 10^{-4}$	0.350 ± 0.009			
Ramos et al., 1988 [13]	$Mn_pZn_{1-p}F_2$ $p = 0.40;\ 0.55;$ 0.83	LB	10^{-2} ?				-0.09 ± 0.03
Ferreira et al., 1991 [14]	$Fe_pZn_{1-p}F_2$ $0.31 \leqslant p \leqslant 0.84$	LB	?				-0.09
Belanger et al., 1995 [15]	$Fe_pZn_{1-p}F_2$ $p = 0.5$	NS	$< 10^{-1}$	0.35			
Belanger et al., 1996 [16]	$Fe_pZn_{1-p}F_2$ $p = 0.52$	NS	10^{-2}	0.35			
Hill et al., 1997 [17]	$Fe_pZn_{1-p}F_2$ $p = 0.5$	XS	10^{-2}	0.36 ± 0.02			
Slanic et al., 1998 [18]	$Fe_pZn_{1-p}F_2$ $p = 0.93$	LB	?				-0.10 ± 0.02
Slanic , 1998 [19]	$Fe_pZn_{1-p}F_2$ $p = 0.93$	NS	?		1.35 ± 0.01	0.71 ± 0.01	
Slanic et al., 1999 [20]	$Fe_pZn_{1-p}F_2$ $p = 0.93$	NS	$10^{-2} - 1.14 \times 10^{-4}$		1.34 ± 0.06	0.70 ± 0.02	

* The experimental techniques are given in the following notations: NMR, nuclear magnetic resonance; LB, linear birefringence; NS, neutron scattering; MS, Mössbauer spectroscopy; SMXS, synchrotron magnetic x-ray scattering; and XS, X-ray scattering. τ denotes a reduced temperature interval, where the power-law fit to the experimental data was carried out or a minimal value of the reduced temperature reached in the experiment.

nonmagnetic isomorph ZnF_2 for FeF_2 (MnF_2). Experiments on the critical behavior of random systems are extremely sensitive to the sample quality. Macroscopic nonstatistical gradients in concentration cause a variation of T_N through the sample, smearing out the sharp transition. Asymptotic critical behavior is observable only very close to T_N. Therefore, to provide a satisfactory realization of random substitution of nonmagnetic ions (Zn^{+2}) for magnetic ones (Fe^{+2}, Mn^{+2}), mixed crystals $Fe_pZn_{1-p}F_2$ as well as $Mn_pZn_{1-p}F_2$ should be grown so as to provide a very low degree of mosaicity, high chemical homogeneity, and, especially, small impurity concentration gradients. The last can be achieved by choosing the impurity concentration from the condition [89] $dT_N/dp = 0$, or on the basis of geometric considerations, taking into account that gradients are usually parallel to the growth axis. Already early experimental studies on the critical behavior of disordered crystals [90, 91] proved the crucial role of sample quality; high-quality samples allowed the observation of sharp phase transition and the measurement of the dependence of the Néel temperature T_N on p via the linear birefringence method [92]. This provided a basis for measurements of universal critical properties. The earliest experimental study of the critical exponents governing the sharp transition at a weak quenched dilution was the nuclear magnetic resonance measurement of magnetization in $Mn_{0.864}Zn_{0.136}F_2$ [4]. The magnitude of the magnetization exponent β was found to differ strongly from that in the undiluted sample (see Table 1).

In two years, the study of Ref. [4] was corroborated by measurements of the staggered susceptibility and the correlation length in an iron-based crystal with a concentration $p = 0.5$ (a high-dilution regime). The experiment was done in a two-axis spectrometer using the neutron scattering technique [5]. The smearing effects were eliminated by masking the crystal to expose only a small homogeneous region. The relative temperature control to about 0.01 K at the substance's Néel temperature of 42.50 K allowed the attainment of an accuracy $\delta|\tau| \sim 5 \times 10^{-4}$ for the reduced temperature. The data for the inverse correlation length and the inverse staggered susceptibility were fit to power laws with critical amplitudes and exponents as free parameters. The power law was shown to be satisfied well within $10^{-3} - 2 \times 10^{-1}$ with the same critical exponents (see Table 1) below and above T_c while differing strongly from those of the pure Ising model. To support the result, caloric properties were measured, too. The fact that for transition-metal difluorides the temperature derivative of the linear birefringence is proportional to the magnetic specific heat within $|\tau| < 10^{-1}$ [92, 93] served as a basis for the experimental technique applicability. Measurements of the critical exponent α were performed on an $Fe_{0.6}Zn_{0.4}F_2$ sample with $T_N = 47.05$ K. In order to minimize the effect of concentration gradients, the laser beam was oriented perpendicularly to the concentration gradient. The numerical value of the critical exponent was extracted by fitting the data to the temperature integral of the specific-heat scaling function taking into account correction-to-scaling terms [i.e., the first two terms in expansion (3)]. In contrast to the pure Ising case, the data obtained yielded $\alpha < 0$ (see Table 1). Within the whole region at reduced temperature τ, neither evidence of pure Ising behavior nor a crossover from pure to random fixed-point critical behavior was found. It was concluded that either the crossover is outside the critical region or it is too smooth. In concluding, let us note that the data obtained in Ref. [5] on the basis of two different substances and quite different experimental procedures proved the correctness of the scaling relation $d\nu = 2 - \alpha$ and thus served as direct experimental support of scaling in dilute systems.

With the typical energy of the neutron beam of about 10 meV, the neutron scattering measurements appeared to be one of the most useful methods for studying the critical region. However, the method turned out to be very sensitive to the samples' quality, since their typical sizes were less than several millimeters. The scattering data contain contributions from transverse and longitudinal spin fluctuations, which have to be separated in a detailed data analysis. This explains why in the measurements of Ref. [7], which were performed on $Fe_pZn_{1-p}F_2$ with concentration 0.46, special attention was paid to the quality of the sample. The variation of 2×10^{-4} in the concentration over the entire volume that was achieved in the study permitted scattering studies within the temperature limits $|\tau| \geqslant 10^{-3}$. Within the interval $1.5 \times 10^{-3} \leqslant |\tau| \leqslant 10^{-1}$, the inverse correlation length was obtained from the width of the Lorentzian fits as a function of temperature, and the correlation length exponent was extracted from the power-law fits. In order to obtain the exponent γ, χ data were extrapolated to the wave vector length $q = 0$ (see Table 1) and the fit to the power-law ansatz was done taking into account the background term. An alternative Mn-based substance ($Mn_pZn_{1-p}F_2$) was studied by neutron scattering a year later [9]. The sample with $p = 0.75$ had an overall spread in concentration of 0.001, which allowed the researchers to perform measurements up to $|\tau| \sim 4 \times 10^{-4}$ (Fig. 3). The $p = 0.5$ sample was of lower quality, with a spread in concentration of 0.005. The high quality of the samples, as well as the temperature control up to 0.05 K, allowed the researchers to obtain critical amplitudes ratios and exponents with good accuracy. However, systematic errors, which were assumed to be due to the resolution corrections, the quasi-

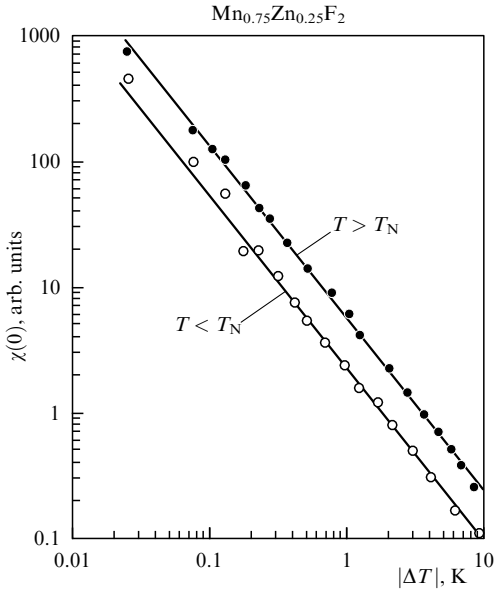

Figure 3. Neutron scattering measurements of $\chi(0)$ in $Mn_{0.75}Zn_{0.25}F_2$ [9]. The solid lines represent a simple power-law dependence obtained by a fit of its parameters to experimental data with the result $\gamma \simeq 1.364$ above and below Néel temperature T_N. The critical behavior is governed by RIM asymptotic critical exponents within the reduced temperature interval $4 \times 10^{-4} < |\tau| < 2 \times 10^{-1}$. The figure is taken from Ref. [9].

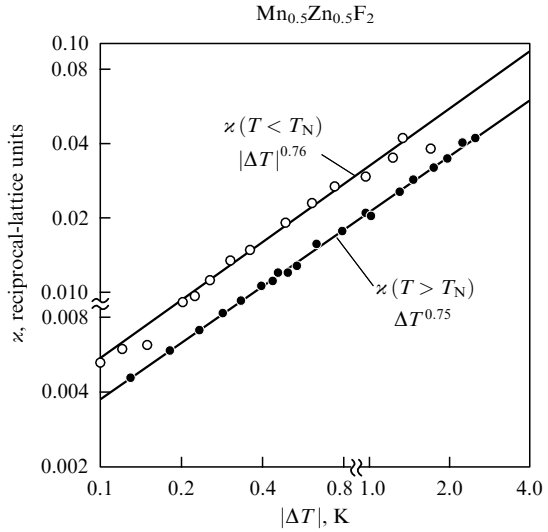

Figure 4. Neutron scattering measurements of the longitudinal inverse correlation length $\varkappa$ in $Mn_{0.5}Zn_{0.5}F_2$ above and below T_N. The solid lines represent a simple power-law dependence obtained by a fit of its parameters to experimental data with the result $\nu' \simeq 0.76$ for $T < T_N$ and $\nu \simeq 0.75$ for $T > T_N$. The data permit the conclusion that $\nu' = \nu$ within the limits of errors (see Table 1). The power-law dependence holds within the reduced temperature interval $5 \times 10^{-3} < |\tau| < 10^{-1}$. The asymptotic region is not reached yet and the obtained exponents are effective. The figure is taken from Ref. [9].

elastic approximation, concentration fluctuations, and background effects, appeared to be of more importance than statistical ones. The authors stressed that, since no correction-to-scaling terms were used, the exponents found are effective. Nonetheless, the $p = 0.75$ sample was shown to exhibit RIM critical behavior over the entire reduced-temperature interval $4 \times 10^{-4} < |\tau| < 2 \times 10^{-1}$; the critical exponents at higher dilution $p = 0.5$ have not reached their asymptotic RIM values (see Table 1 and Fig. 4).

The aforementioned results obtained for single crystals of transition-metal fluorides were corroborated [6] by neutron scattering experiments on a sample of $Dy_3Al_5O_{12}$ powder. A powder of this cubic noncollinear Ising antiferromagnet, together with nonmagnetic yttrium, was prepared to avoid gradients in a composite sample, where they usually occur. The critical exponent β increased in a disordered sample in comparison to the value of the 'pure' Ising model (see Table 1) and provided extra evidence of the conformity between experiment and theoretical predictions.

It is known that static critical behavior of a diluted Ising magnet in a uniform field H corresponds to the random-field Ising model [94, 95]. This model is the subject of recent intensive experimental studies (see [2, 96]). Two works on neutron scattering measurements in RIM appeared in the middle of the 1990s in the context of studies of random-field model properties [15, 16]. In the experiments the problem of the Bragg scattering saturation due to extinction effects was partially solved by growing a 3.4-μm epitaxial film of $Fe_{0.5}Zn_{0.5}F_2$ on a (001) ZnF_2 substrate. The small X-ray rocking curve linewidth of the (001) reflection showed the film to be of very high quality, which was in part due to the nearly identical lattice parameters a of the substrate and substance. On the other hand, since the film thickness was 10^4 lattice spacings, the film could be considered as a three-dimensional object. This was proven in experiments on FeF_2, where the critical behavior of the 'pure' $d = 3$ Ising magnet was observed [97]. The transverse (100) Bragg scattering scan data appeared to be well described by a Gaussian distribution with a background term. Fitting the Bragg amplitude vs. temperature to a simple power law, a critical exponent $\beta = 0.35$ was found for $H = 0$. However, a smoothing-off of the expected critical behavior of the magnetization near T_N prevented an accurate analysis of the data. To reveal whether this was caused by poor sample quality, measurements on the 3.4-μm film of $Fe_{0.52}Zn_{0.48}F_2$ were performed [16]. The higher resolution data confirmed the obtained value of β and showed that smoothing-off was only due to insufficient resolution. Recently in neutron scattering studies of a crystal 0.44 mm thick, the region of investigation was extended from $|\tau| \geqslant 10^{-2}$ to $|\tau| \geqslant 10^{-4}$, which allowed obtaining the correlation length and susceptibility critical exponents [19, 20].

The Mössbauer spectroscopy studies of critical behavior started in 1986 on a class of Fe-based substances with various concentrations of magnetic atoms [8]. The method was tested earlier for the 'pure' Ising antiferromagnet FeF_2. It had been shown that the sublattice magnetization is proportional to the field h, which can be measured in Mössbauer spectroscopy [88]. To apply the approach to a dilute magnet, the variation of the concentration of Zn was reduced to 10^{-4}, and a temperature stability of 0.002 K was achieved. In order to fix the critical temperature, the values of β were chosen such that the plot $h(T)^{1/\beta}$ vs. T became a straight line intersecting the abscissa axis at T_N. This method appeared not to be sensitive to particular values of β and gave an accuracy of 0.05 K for the critical temperature location. Though the critical exponent β can be obtained from the curve slope in a double-logarithmic plot, this method produced results only after separating the data into two intervals in τ, which were characterized by obviously different critical exponents: one of the 'pure' Ising model and the other of RIM. The crossover in β occurred within a very narrow range and at relatively large values of τ ($10^{-1} \geqslant |\tau| \geqslant 10^{-3}$) for small dilutions ($p \geqslant 0.95$). Subsequent studies using Mössbauer spectroscopy appeared two years later [11] and were characterized by a very detailed analysis of the data. Their advantage was a high quality of the sample grown from a stoichiometrical mixture of FeF_2 and ZnF_2 powders, each prepared by reacting a metal sponge with dry HF at +900 °C. In the experiment the concentration gradients in a single crystal absorber were minimized by choosing the direction of the γ ray parallel to the growth axis, which was perpendicular to the plane of the sample disk; the exposed area was $4 \times 5 \times 0.1$ mm. Twenty constant-acceleration spectra were obtained within $3 \times 10^{-4} < |\tau| < 0.86$. Very good temperature stability, 3 mK day^{-1}, and taking into account corrections to scaling permitted the obtainment of the asymptotic RIM magnetization critical exponent β from the data within the whole investigated interval (see Table 1).

The optical linear birefringence method introduced in Ref. [5] for the study of critical behavior of the magnetic part of the specific heat c_m in disordered magnets was further developed in Refs [13, 14, 18]. A proportionality between the temperature derivative $d(\Delta n)/dT$ of the optical birefringence Δn and c_m is assumed for optically transparent materials. Though the caloric properties in the critical region can also be measured by a pulsed heat technique, the optical linear birefringence method has several advantages. First, the nonmagnetic contribution of the optical birefringence to the temperature derivative is insignificant, contrary to thermal

techniques, where the nonmagnetic phonon background is often large and difficult to eliminate. Second, one can minimize the concentration fluctuation effects by applying a laser beam perpendicularly to the concentration gradients. In the first experiment [13] on a class of single crystals with various impurity concentrations, it was shown that the exponent α is independent of the concentration and is in very good agreement with the theoretical predictions (see Fig. 5, as well as Section 4). Two subsequent studies [14, 18] showed the equivalence of the method with direct heat pulsing measurements. Magnetic X-ray scattering successfully applied to the 'pure' Ising crystal [98] was applied to the 'random' Ising crystal for high dilution in Ref. [10]. For samples of size $5.7 \times 6.4 \times 8.9$ mm of good crystallographic quality (low mosaicity) the mean-field value of the exponent β was found up to $|\tau| \leqslant 0.06$, while closer to T_N an exponent β consistent with the RIM value was obtained.

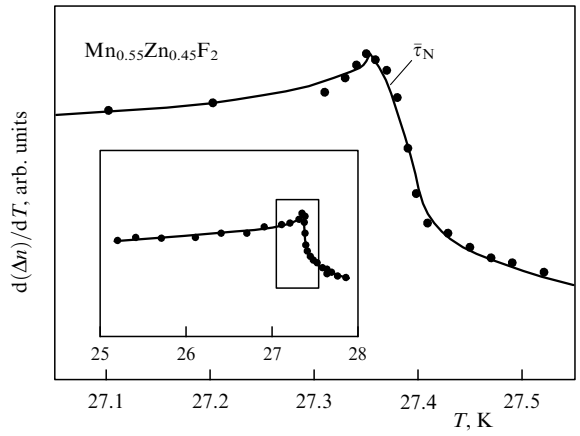

Figure 5. The temperature derivative of the optical birefringence of $Mn_{0.55}Zn_{0.45}F_2$ at zero magnetic field. The main part of the figure presents the data for $d(\Delta n)/dT$ in the critical region (shown by a box in the inset). The measurements attest to a cusplike behavior of the RIM specific heat with a critical exponent $\alpha = -0.09 \pm 0.03$. The figure is taken from Ref. [13].

4. Monte Carlo simulations

The power-law singularities of physical quantities [see, e.g., Eqn (1)] appear only in the thermodynamic limit, when the system volume and the number of particles tend to infinity. Therefore, an obvious obstacle in computer 'experiments' is that simulations can be done for a system of finite size only. Moreover, in the computer 'experiments' the asymptotic temperature interval fails to be reached, since T_c itself does not exist for finite systems. However, the location of the critical temperature is crucial for the accuracy of determination of critical exponents. One can extrapolate data to the thermodynamic limit assuming that the regime of a constant asymptotic critical exponent is already established starting from a certain finite system size and within an interval around T_c of a certain nonzero size. The last assumption exploited in computer simulations leads to a very narrow temperature interval below and above T_c reliable for data sampling. The upper bounds are the temperatures where corrections to scaling are taken into account. The lower bound follows from finite-size effects and is of an order of 10^{-3} for typical system sizes achieved now in Monte Carlo (MC) simulations. Therefore, the exponents obtained in the manner described are often effective critical exponents which characterize the critical behavior in the observable temperature range. On the other hand, the dynamic behavior of pure and disordered spin systems is governed by different time scales. Thus, only very long-running simulations yield reliable data in the latter case. The relaxation time increases drastically not only when approaching T_c. In early simulations it also increased with the dilution; as a result, for several decades higher values for relaxation times were obtained when passing from a pure $p = 1$ system to a diluted one with $p = 0.6$. However, application of a more elaborate simulation technique resulted in an opposite behavior: a decrease of the relaxation time for a certain disordered sample with an increase of p [99]. It is the configurational averaging that leads to an overall increase in the computation time. The statistical errors for thermodynamic observables result mainly from variance in configurational space and are larger than usual statistical errors in finite-size simulations with what are now usual statistics of 10^6 MCS (Monte Carlo steps per spin). Consequently, the accuracy is bounded by the available CPU time on the one hand and limited by the number of samples to perform the configuration averaging in a disordered model [75] on the other hand. Efficient algorithms, together with high-speed computers, partially solve the task.

Despite the complicated situation, Monte Carlo studies provided deep insight into the origin of the phase transition in the RIM as well as resulted in reliable numerical values for the critical exponents. MC studies of the three-dimensional RIM systems have been carried out over the last two decades [21–40]. The first search [21] for universal critical characteristics of RIM was performed on a simple cubic lattice of a size 30^3 using the importance-sampling MC method [100]. The positions of specific heat peaks corresponding to finite-lattice pseudo-critical temperature were extrapolated to T_c by means of finite-size scaling theory. The achieved accuracy of 500–5000 MCS per data point and averaging over several different starting configurations of impurities did not allow the researchers to discriminate between disorder relevance or irrelevance. The data analysis revealed that values of the order-parameter exponent β and the susceptibility exponent γ of RIM could not be distinguished (within the error bars) from the corresponding exponents of the pure system for any dilution (see Table 2, Ref. [21]). As a possible explanation, it was stated that the lattice studied was too small to reach the critical region. Thus, 'impure' critical behavior can be observed only for systems with larger critical regions (larger value of α_{pure}). This assumption was refuted by MC simulations of RIM on larger lattices, higher statistics (5000–11000 MCS), larger numbers of averaged samples, and a more detailed analysis of simulation data, however within a narrower dilution range [22]. The location of the phase-transition temperature T_c was determined from the data on the specific heat and the numerical derivative of the energy. In this way, the accuracy of critical temperature determination was improved to 0.004. Finally, the processing of magnetization data permitted concluding the relevance of disorder for the universal critical properties of RIM. However, the critical exponent β was found to vary continuously with the magnetic-site concentration. It was also found that no temperature region with a constant value of β exists. Similarly to Ref. [21], the authors of Ref. [22] stressed that, while they cannot exclude the existence of a tiny 'impure' critical region, it is unobservable for the weak dilution, both

Table 2. The critical exponents of RIM obtained in MC simulations (the asterisk at the concentration value denotes that disorder was realized in a canonical manner).

References	Maximum size	Concentration interval	p	β	γ	ν
Landau, 1980 [21]	30	$0.4 < p \leqslant 1$	all	0.31	1.25	
Marro et al., 1986 [22]	40	$0.8 \leqslant p \leqslant 1$	1 0.985 0.95 0.9 0.8	0.30 ± 0.02 0.31 ± 0.02 0.32 ± 0.03 0.355 ± 0.010 0.385 ± 0.015		
Chowdhury et al., 1986 [23]	90	$0.8 \leqslant p \leqslant 1$	1 0.95 0.90 0.80	0.29 ± 0.02 0.28 ± 0.02 $0.31 \pm 0{,}02$ 0.37 ± 0.02		
Braun et al., 1988 [24]	40		0.80	0.392 ± 0.03		
Wang et al., 1989 [26]	100	$0.4 \leqslant p \leqslant 0.8$	все		1.52 ± 0.07	0.77 ± 0.04
Wang et al., 1990 [27]	300		0.8		1.36 ± 0.04	
Holey et al., 1990 [28]	64	$0.8 < p \leqslant 1$	1 0.9 0.8			0.629(4) $< 2/3$ 0.688(13)
Heuer, 1990 [29]	60	$0.5 < p \leqslant 1$	1 0.9 0.8 0.6 0.5	0.305 ± 0.01 0.315 ± 0.01 0.330 ± 0.01 0.330 ± 0.01 0.335 ± 0.01	1.24 ± 0.01 1.30 ± 0.01 $1.35 \pm 0{,}01$ 1.48 ± 0.02 1.49 ± 0.02	
Heuer, 1993 [30]	60	$0.6 < p \leqslant 1$	1 0.95 0.9 0.8 0.6	0.33 ± 0.01 0.31 ± 0.02 0.31 ± 0.02 0.35 ± 0.02 0.33 ± 0.02	1.22 ± 0.02 1.28 ± 0.03 1.31 ± 0.03 1.35 ± 0.03 1.51 ± 0.03	0.624 ± 0.010 0.64 ± 0.02 0.65 ± 0.02 0.68 ± 0.02 0.72 ± 0.02
Hennecke et al., 1993 [32]	90		0.6	0.42 ± 0.04		0.78 ± 0.01
Wiseman et al., 1998 [34]	64		0.8	0.344 ± 0.003	1.357 ± 0.008	0.682 ± 0.003
Wiseman et al., 1998 [35]	90 80		0.6^* 0.6	0.316 ± 0.013 0.313 ± 0.012	1.522 ± 0.031 1.508 ± 0.028	0.722 ± 0.008 0.717 ± 0.007
Ballesteros et al., 1998 [33]	128	$0.4 \leqslant p \leqslant 0.9$	all	0.3546 ± 0.0028	1.342 ± 0.010	0.6837 ± 0.0053
Marques et al., 2000 [38]	60	$0.8 \leqslant p \leqslant 0.9975$	all	0.3546	1.342	
Marques et al., 2000 [39]	100	0.5				0.6837

experimentally and within the Monte Carlo method. As a result, effective critical exponents varying continuously with dilution would always show up according to the two-fixed-points scenario (see Fig. 2). The possibility of the existence of a line of fixed points, one for each impurity concentration, is not excluded either (compare the dependence of the magnetization critical exponent β on the concentration of magnetic sites in Table 2, Ref. [22]).

The results mentioned above appeared to be in good agreement with the MC data of Ref. [23] obtained on the basis of a multispin coding program. Though systems twice as large and 8000 MCS statistics were used for a given concentration and temperature, the effective exponent β was found to increase continuously with dilution as well. Such a behavior of β was explained by the fact that the equilibrium magnetization was calculated too far from the critical point. Two years later, the conclusion that reliable critical exponent values could not be obtained by the simulation of systems with sizes $l \leqslant 20$ was drawn in Ref. [24]. Statistical errors in the determination of the critical temperature from susceptibility and/or specific heat data, together with the extrapolation by finite-size scaling were thought to be responsible for this situation. In particular, corrections to scaling [101] needed to be taken into account. Instead, the simulation with a statistics of 5000 – 11000 MCS but without configuration averaging, allowed the determination of the exponent β.

The value obtained turned out to be evidently larger than the corresponding value in the 'pure' case. Simultaneously, due to a large scatter of the data, a determination of the exponent γ was not done. A reanalysis of the previous MC simulations [21–23] led the authors of [24] to the conclusion that a large part of the critical regime is dominated by the crossover from pure Ising to RIM exponents: the results of Ref. [21] may correspond to a plateau value of the effective critical exponent governed by the pure Ising fixed point. Similarly, the results of Refs [22, 23], after refined analysis, correspond to an intermediate regime near T_c before the unaccessible asymptotic region. Exploiting the concept of effective critical exponents [68, 69] [see formula (2)], the authors of Ref. [24] claimed that the effective exponents they found were in qualitative agreement with the renormalization-group flows (see Fig. 2).

It soon became clear that the concentration dependence of the critical exponents observed previously in MC simulations is due to the large relaxation time at criticality. The application of the Swedsen–Wang algorithm to RIM simulation [26] resulted in the conclusion that the analysis of the susceptibility data within the finite-size scaling method is not adequate to check whether new critical exponents appear in RIM. The conclusion was based on the observation that the ratio γ/ν does not change with system size. On the other hand, the determination of T_c from the susceptibility maximum on the base of the fourth-cumulant intersection method permitted the calculation of the effective critical exponent γ by analysing the data in successive time intervals. In this way, the susceptibility and the correlation-length critical exponents were found to be independent of concentration in a wide range of dilutions (see Table 2, Ref. [24]). As observed in Ref. [26], the exponent γ is higher than the theoretical asymptotic value. Thus, it was found that γ_{eff} is a nonmonotonic function of reduced temperature with a maximum value that is the larger, the bigger the dilution. For the particular case of magnetic sites of concentration 0.8, the prediction was investigated in Ref. [27] by the Swedsen–Wang algorithm and the single-cluster generalization of Wolf for rather large systems. While the γ/ν ratio confirmed the result of Ref. [26], a maximum of the effective critical exponent γ when approaching T_c was not observed.

The assumption that the interaction among block-spins in diluted systems may be represented by renormalized couplings of pure systems was used in the MC renormalization-group approach for RIM in the weak-dilution region ($p \geqslant 0.8$) [28]. The values for the correlation-length critical exponent ν were found to depend on the concentrations of the magnetic sites. For $p = 0.8$, the exponent ν satisfied the exact inequality $\nu > 2/d$ for a diluted system [72]. This led the authors of Ref. [28] to the assumption that they obtained an asymptotic value of the critical exponent. At the mentioned concentration of magnetic sites, the authors estimated the width of the asymptotic critical region ($|\tau|_{\text{crit}} \leqslant 3 \times 10^{-4}$) where no influence of the fixed point of the pure Ising model is observed. Alternatively, for $p = 0.9$ the inequality for ν [72] was not satisfied. Thus, either the critical region $|\tau|_{\text{crit}} \leqslant 1.3 \times 10^{-4}$ was not reached and the critical behavior of the pure Ising model was observed, or the crossover to the RIM asymptotic critical behavior for $p = 0.9$ is observable only in larger systems. For $p = 0.4$, the accuracy of the data obtained was too poor to draw any conclusions.

Reliable data obtained within the Monte-Carlo method in Ref. [29] became possible after the application of a new cluster algorithm [102] and a refined vectorized implementation of local algorithms [103]. A progress in MC studies occurred when an improved version of the multispin coding program appeared [29, 103]. It allowed the researchers to verify all previously obtained simulation data for RIM with the unprecedented statistics of up to 3×10^5 MCS and 10 averaged configurations for systems with $p \geqslant 0.8$ and up to 1.2×10^6 MCS for higher dilutions. For instance, in the test simulation, the above statistics permitted obtaining the susceptibility and magnetization critical exponents of a two-dimensional pure Ising model with an accuracy of 1% and 3%, respectively. For RIM, the effective exponents γ, β, and $\zeta = 1 - \beta$ (the last one describes the divergence of the magnetization–energy correlation function) [29] were shown to be concentration-dependent in the concentration region $0.5 \leqslant p < 1$ (see Table 2). The value of T_c, as well as of γ, was obtained by fitting susceptibility data to a simple power law; the T_c location was then verified by the 4th and 6th cumulant of magnetization. The investigation of the energy–magnetization correlation function enabled the researchers to check whether scaling holds; the critical exponents ζ and β were obtained by fitting the data to a simple power law with a value T_c taken from the susceptibility analysis. All data showed power-law behavior within the chosen temperature range, but the values of critical exponents changed with concentration (see Fig. 6). For instance, the values of γ and β increased from the pure Ising value and smoothly changed with dilution, achieving a plateau value at $p = 0.5$. Simultaneously, the value of ζ decreased in such a way that the sum of ζ and β was equal to 1 within the limit of errors. The conclusion of Ref. [29] was that while new critical exponents that change with the dilution were observed, no line of stable fixed points exists as supposed, in particular, in Ref. [22]. A conjecture was expressed that such a behavior originates from the crossover from a pure to a diluted regime, as well as from a percolation regime to a diluted one with effective exponents for all concentrations.

The evidence of crossover phenomena motivated the authors to undertake a more systematic study. The data of Ref. [29] were revised three years later in Ref. [30] where a cumulant method was used in order to determine T_c. For thermal averaging, up to 40000 MCS were performed, and for configurational averaging, up to 32 configurations were used (compare this with 5000 MCS and only several samples for

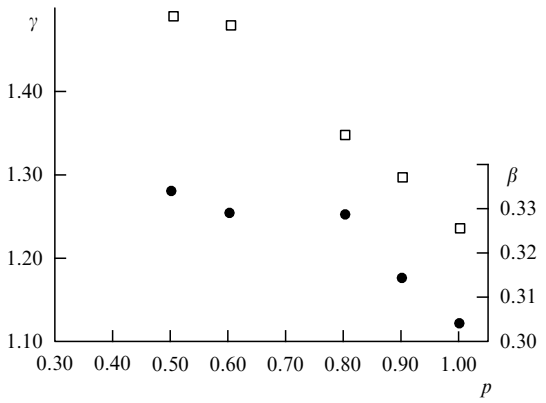

Figure 6. RIM effective critical exponents β (solid circles) and γ (squares) for different dilutions p obtained in MC simulations [29]. All exponents change continuously with dilution and are clearly different from the pure Ising values. The figure is taken from Ref. [29].

the configurational average in Ref. [21]). The critical exponents ζ, β, and γ were shown to vary with concentration in consistency with the two-fixed-point scenario for the weak dilution. However, for the strong dilution ($p = 0.5$; 0.6) an influence of a different 'percolative' fixed point was assumed. A central part of Ref. [30] dealt with the magnetization – energy scaling function. It was shown that dilute systems exhibit a complex crossover behavior before they reach an asymptotic critical region with the values of the exponents consistent with the weak random fixed point, while pure systems reach their asymptotic limit for small sizes. In weakly random systems ($p \geqslant 0.8$), the asymptotic values for the exponents are smoothly approached from below, whereas in strongly diluted systems they are approached from above. The asymptotic values of the exponents are reached at a characteristic system size λ_p that depends on the concentration p. According to the estimates performed, the value of λ_p is on the order of 20 – 30 lattice constants for pure systems, 50 at $p = 0.95$ and 0.9; about 100 – 150 at $p = 0.6$; and diverges at the percolation point. Thus, more strongly disordered systems necessitate a refined analysis with an appropriate treatment of their percolative structural effects relevant for nonasymptotic sizes and correlation lengths. Due to presently unknown reasons, the crossover function changes its sign at $p \sim 0.8$, so the asymptotic values appear to be reached already for small systems (cf. Refs [27, 29]).

Due to works [26, 27] and especially [29, 30], it became clear that the concentration-dependent critical exponents found in MC simulations are effective, characterizing the approach to the asymptotic region. This point of view found its support in a conjecture about a steplike universality of the three-dimensional diluted magnets [31]. An attempt to study the diluted model at $p = 0.6$ by means of taking MC data from different subsystems of one large system was made in Ref. [32]. It was concluded that the resulting values of the critical exponents are strongly influenced by the size of the system. Recently, the critical behavior of the RIM was reexamined by the MC method in Ref. [33] for $0.4 \leqslant p \leqslant 0.9$ and in Refs [34, 35] for concentrations $p = 0.8$ and 0.6. In particular, the simulations performed in Ref. [35] revealed that a disorder realized in a canonical manner (by fixing the fraction of magnetic sites) leads to different results in comparison with disorder realized in a grand-canonical manner (see Table 2). Studies of Ref. [33] were based on the importance of taking into account the leading correction-to-scaling term in the infinite volume extrapolation of the MC data and, thus, the analysis does not agree with the data of Ref. [35]. The results of the simulations for the concentrations $p = 0.9$, 0.8, 0.6, and 0.4 were extrapolated to an infinite system size (see Fig. 7) and led to the proof of universal critical behavior of the site-diluted Ising model in a wide range of concentrations. In particular, the value of the correction-to-scaling exponent ω was found to be $\omega = 0.37 \pm 0.06$, which is almost half as large as the corresponding value in the pure $d = 3$ Ising model ($\omega = 0.799 \pm 0.011$) [73]. The smaller the value of ω, the larger the interval where it has to be taken into account [cf. formula (3)]. Thus the smallness of ω in the dilute case explains its importance for an analysis of the asymptotic critical behavior.

Another important question considered in Refs [34, 35] was the problem of self-averaging in RIM. The Gibbs approach to static collective phenomena rests on the statistical independence of macrosamples according to the short-range nature of interparticle interactions. In agreement

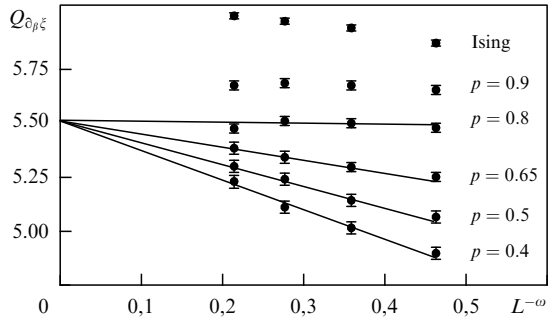

Figure 7. Determination of the correction-to-scaling exponent ω in MC simulations of Ref. [33]. The quantity $Q_{\partial_p \xi} = 2^{1+1/\nu}$ is plotted for different dilutions $0.4 \leqslant p \leqslant 1$ and lattice sizes $8 \leqslant L \leqslant 128$. One can see that at $p = 0.9$ the system passes from a regime of the fixed point of the pure Ising model to that of the diluted model even for $L = 128$. The solid lines correspond to a fit $\omega = 0.37$ providing the same infinite volume extrapolation for all $p \leqslant 0.8$. The figure is taken from Ref. [33].

with this approach, any thermodynamic extensive quantity M is (strongly) self-averaging. This means that the normalized square width R_M of the squared variance of its subsystem values behaves as $R_M \sim 1/n \sim l^{-d}$, where n is the number of subsystems and l is the system linear size. However, in the vicinity of the critical point the statistical independence does not hold, since the correlation length of a system ξ can be arbitrarily large ($\xi \sim l$), and thus subsystems cannot be considered as independent. The concept of weak self-averaging corresponds to the case where a number x_1 ($0 < x_1 < d$) exists such that R_M at criticality scales as l^{-x_1}. On the contrary, if $R_M \to \text{const} \neq 0$, M is called non-self-averaging. It has been predicted on the basis of heuristic arguments that for random models all extensive quantities are strongly self-averaging far from criticality. Yet for a quantity M, which scales as l^{ρ} at the critical point, the strong self-averaging should fail. Here, the squared variance V_M is expected to scale as $l^{2\rho+\alpha/\nu}$ for $\alpha_{\text{random}} < 0$ assuming $R_M \sim l^{\alpha/\nu}$ or weak self-averaging [104].

Lack of self-averaging in RIM is not only of high theoretical interest. The reliability of MC simulations depends on whether an increase of the lattice size improves the statistics of the simulations. If a quantity is non-self-averaging, the simulational data are unreliable. Theoretical studies based on the renormalization-group approach confirmed the strong self-averaging for $l \gg \xi$. In contrast, special MC investigations in finite systems found no self-averaging in the case of a significant disorder $\alpha_{\text{pure}} > 0$. It appeared that weak self-averaging is the case only for insignificant disorder [105], in disagreement with Ref. [104]. The MC simulations of Refs [34, 35] were performed in order to solve this problem. It was shown that the normalized square width R_M goes to a constant for large l, which is independent of the dilution of the grand-canonical type. For the canonical type of dilution, this is not the case [34]. The last result, however, may have its explanation in a very slow approach of R to its universal asymptotic value, estimated as $l^{\alpha/\nu}$ [36], in the case of the canonical realization of disorder in RIM.

The evolution of the self-averaging from pure Ising model to RIM has been studied recently [37] in order to determine the transition zone between the universality classes of pure and diluted Ising models. It was shown that the transition zone is smoothly dependent on the concentration of magnetic

sites and independent of the lattice size. On the contrary, critical exponents did not depend on concentration and were found identical to the data of Ref. [33]. The universal value of the normalized square width of the susceptibility in the infinite-volume limit was estimated to equal $R_\chi(\infty) = 0.155$.

Apart from short-range site dilution, other realizations of disorder have become the subject for MC simulations recently. The thermally diluted Ising model has been studied as a generalization of the RIM [38, 39]. There, the realization of the vacancy distribution is determined from the local distribution of spins in a pure Ising model at criticality. The critical properties, in particular, the universality class of the model, appeared to differ strongly from the RIM one and better agree with the theoretical predictions for long-range-correlated disorder. [3]

The problem of whether the RIM fixed point also describes the phase transition in the Ising model with random bonds has been studied explicitly in Refs [40, 41]. Using a numerical renormalization-group analysis, the renormalization-group (RG) flows for random Ising models have been obtained. The existence of a fixed point characterizing the random Ising model irrespective of the type of disorder has been shown [40].

5. Renormalization-group-theory expansions

In Sections 5 and 6, we will review results on RIM critical exponents obtained my means of renormalization-group (RG) methods. In Section 5, we will report the main relations of the field-theoretical RG approach and dwell upon perturbation-expansion series available. In Section 6, we will consider the RG series resummation methods and discuss the results obtained on their basis.

5.1 Renormalization

To theoretically describe the long-distance properties arising in different systems in the vicinity of a second-order phase transition point, it is now standard to use a field-theoretical RG approach [108, 109]. The renormalization is used to remove divergences that occur during evaluation of the bare vertex functions in the asymptotic limit. For RIM, one-particle irreducible bare vertex functions are defined as

$$\begin{aligned}\delta(q_1 + \ldots + q_N)\, \Gamma_0^N(q_1, \ldots, q_N;\, m_0, u_0, v_0;\, \Lambda_0) \\ = \int \exp\left\{\mathrm{i}(q_1 r_1 + \ldots + q_N r_N)\right\} \\ \times \left\langle \varphi(r_1) \ldots \varphi(r_N)\right\rangle_{1\mathrm{PI}}^{\mathcal{H}_{\mathrm{RIM}}} \mathrm{d}r_1 \ldots \mathrm{d}r_N\,, \end{aligned} \tag{12}$$

where the angular brackets denote the statistical average over the Gibbs distribution with Hamiltonian (8) in the replica limit $n \to 0$, and the subscript 1PI indicates that only one-particle irreducible diagrams are taken into account. The functions depend on the set of momenta $q_1, \ldots, q_N$ (with Λ_0 as a momentum cutoff) and the bare parameters m_0, u_0, v_0 of the Hamiltonian (8). Divergences in (12) occur in the asymptotic limit $\Lambda_0 \to \infty$. Their removal is achieved by a controlled rearrangement of the series for the vertex functions. Several asymptotically equivalent procedures serve this purpose. We will use two complementary approaches: (a) dimensional regularization and the minimal-subtraction scheme [110] and (b) the fixed-dimension renormalization at zero external momenta and nonzero mass (a massive RG scheme) [111].

Let us formulate relations of the renormalized theory. The renormalized fields, mass, and couplings ϕ, m, u, v are introduced by

$$\varphi = Z_\phi^{1/2} \phi\,, \tag{13}$$

$$m_0^2 = Z_{m^2}\, m^2\,, \tag{14}$$

$$u_0 = \mu^\varepsilon\, \frac{Z_{4,u}}{Z_\phi^2}\, u\,, \tag{15}$$

$$v_0 = \mu^\varepsilon\, \frac{Z_{4,v}}{Z_\phi^2}\, v\,. \tag{16}$$

Here, $\varepsilon = 4 - d$; μ is a scale parameter equal to the renormalized mass at which the massive scheme [111] is evaluated or in the minimal-subtraction scheme [110] it sets the scale of the external momenta; and $Z_\phi, Z_{m^2}, Z_{4,u}, Z_{4,v}$ are the renormalizing factors. The renormalized vertex functions Γ_R^N expressed in terms of the bare vertex functions by

$$\Gamma_R^N(q_1, \ldots, q_N;\, m, u, v) = Z_\phi^{N/2} \Gamma_0^N(q_1, \ldots, q_N;\, m_0, u_0, v_0) \tag{17}$$

are finite. This is the main content of the multiplicative renormalizability of the field theory defined by the Hamiltonian (8).

First, let us consider the *minimal-subtraction scheme*. Here, the renormalizing Z factors (13)–(16) are determined by the condition that all poles at $\varepsilon = 0$ are removed from the renormalized vertex functions. The RG equations are written bearing in mind that the bare vertex functions Γ_0^N (12) do not depend on the scale μ, and therefore their derivatives with respect to μ at fixed bare parameters are equal to zero. So, we obtain

$$\mu\, \frac{\partial}{\partial \mu}\, \Gamma_0^N\big|_0 = \mu\, \frac{\partial}{\partial \mu}\, Z_\phi^{-N/2} \Gamma_R^N\big|_0 = 0\,, \tag{18}$$

where the index 0 means differentiation at fixed bare parameters. Then, the RG equation for the renormalized vertex function Γ_R^N reads

$$\begin{aligned}\left(\mu\, \frac{\partial}{\partial \mu} + \beta_u\, \frac{\partial}{\partial u} + \beta_v\, \frac{\partial}{\partial v} + \gamma_m m\, \frac{\partial}{\partial m} - \frac{N}{2}\gamma_\phi\right) \\ \times \Gamma_R^N(m, u, v, \mu) = 0\,, \end{aligned} \tag{19}$$

and the RG functions are given by

$$\beta_u(u, v) = \mu\, \frac{\partial u}{\partial \mu}\bigg|_0\,, \tag{20}$$

$$\beta_v(u, v) = \mu\, \frac{\partial v}{\partial \mu}\bigg|_0\,, \tag{21}$$

$$\gamma_\phi = \mu\, \frac{\partial \ln Z_\phi}{\partial \mu}\bigg|_0\,, \tag{22}$$

$$\gamma_m(u, v) = \mu\, \frac{\partial \ln m}{\partial \mu}\bigg|_0 = \frac{1}{2}\, \mu\, \frac{\partial \ln Z_{m^2}^{-1}}{\partial \mu}\bigg|_0\,. \tag{23}$$

Using the method of characteristics [112], a formal solution of the partial differential Eqn (19) can be written as

$$\Gamma_R^N(m, u, v, \mu) = X(\ell)^{N/2} \Gamma_R^N\big(Y(\ell)\, m, u(\ell), v(\ell), \mu\ell\big)\,, \tag{24}$$

[3] Currently, two possible scenarios for the influence of long-range-correlated disorder on critical behavior are discussed (cf. Refs [106] and [107]). Although both confirm the relevance of long-range-correlated disorder for critical universal properties, they lead to different numerical predictions for the critical exponents.

where the characteristics are the solutions of the ordinary differential equations (flow equations)

$$\ell\frac{\mathrm{d}}{\mathrm{d}\ell}\ln X(\ell)=\gamma_\phi\big(u(\ell),v(\ell)\big)\,,\quad \ell\frac{\mathrm{d}}{\mathrm{d}\ell}\ln Y(\ell)=\gamma_m\big(u(\ell),v(\ell)\big)\,,$$

$$\ell\frac{\mathrm{d}}{\mathrm{d}\ell}u(\ell)=\beta_u\big(u(\ell),v(\ell)\big)\,,\quad \ell\frac{\mathrm{d}}{\mathrm{d}\ell}v(\ell)=\beta_v\big(u(\ell),v(\ell)\big) \tag{25}$$

with

$$X(1)=Y(1)=1\,,\quad u(1)=u\,,\quad v(1)=v\,. \tag{26}$$

For small values of ℓ, Eqn (124) maps the large length scales (the critical region) to the noncritical point $\ell=1$. In this limit the scale-dependent values of the couplings $u(\ell)$ and $v(\ell)$ approach the stable fixed point, provided such a fixed point exists. The fixed points u^* and v^* of the differential Eqns (25) are given by the solutions of the system of equations

$$\beta_u(u^*,v^*)=0,\qquad \beta_v(u^*,v^*)=0\,. \tag{27}$$

The stable fixed point is defined as the fixed point where the stability matrix

$$B_{ij}=\frac{\partial\beta_{u_i}}{\partial u_j}\,,\quad u_i=\{u,v\} \tag{28}$$

possesses eigenvalues ω_1 and ω_2 with positive real parts. The stable fixed point, which is reached starting from the initial values ℓ_0 in the limit $\ell\to 0$, corresponds to the critical point of the system. In the limit $\ell\to 0$ (corresponding to the limit of an infinite correlation length), the renormalized couplings reach their fixed-point values and the critical exponents η and ν are then given by

$$\eta=\gamma_\phi(u^*,v^*)\,, \tag{29}$$

$$\frac{1}{\nu}=2\big(1-\gamma_m(u^*,v^*)\big)\,. \tag{30}$$

In the nonasymptotic region but near the fixed point, deviations from the power laws with fixed-point values of the critical exponents are governed by the correction-to-scaling exponent

$$\omega=\min(\omega_1,\omega_2) \tag{31}$$

in accordance with the Wegner expansion [70] (3). The other critical exponents are obtained by familiar scaling laws [67, 108]

$$\alpha=2-d\nu\,,\quad \beta=\frac{\nu}{2}\,(d-2+\eta)\,,\quad \gamma=\nu(2-\eta)\,, \tag{32}$$

which can be shown to hold from solutions (24).

The flow equations (25) can serve to describe the approach to criticality in a larger region where corrections to scaling do not suffice. As was mentioned in Section 1, out of the asymptotic region physical observables are characterized by effective exponents introduced to describe a crossover from the background behavior to the asymptotic critical one. In the RG language they depend on the flow parameter $\ell(\tau)$ through the dependence of couplings on ℓ. In particular, according to the definition [see formula (2)] for the magnetic susceptibility effective exponent γ_{eff}, we have

$$\gamma_{\mathrm{eff}}(\tau)=-\frac{\mathrm{d}\ln\chi(\tau)}{\mathrm{d}\ln\tau}=\gamma\big(u(\ell(\tau)),v(\ell(\tau))\big)+\dots\,, \tag{33}$$

where the second part is proportional to the β functions and comes from the change in the amplitude part of the susceptibility. It is natural to neglect this part in the vicinity of a fixed point. Moreover, the contribution of the amplitude function to the crossover does seem to be small [113, 114]. Under this restriction, the effective exponents are simply given by the expressions for the asymptotic exponents (29), (30) but replacing the fixed-point values of the couplings u^* and v^* by the solutions of the flow equations (25)

$$\eta_{\mathrm{eff}}(\ell)=\gamma_\phi\big(u(\ell),v(\ell)\big)\,,\quad \frac{1}{\nu_{\mathrm{eff}}(\ell)}=2\big(1-\gamma_m\big(u(\ell),v(\ell)\big)\big)\,. \tag{34}$$

In the *massive RG scheme*, the Z factors (13)–(16) are calculated from the vertex functions (12) at zero external momenta $q_1,\dots,q_N$ and nonzero mass at fixed space dimension in the limit $\Lambda_0\to\infty$. These normalization conditions lead to the equation for the renormalized vertex functions which is known as the *Callan–Symanzyk equation*. Differentiation of the proper bare vertex function Γ_0^N with respect to the renormalized mass [cf. Eqn (18)] gives

$$m\,\frac{\partial}{\partial m}\,\Gamma_0^N\bigg|_0=m\,\frac{\partial m_0^2}{\partial m}\bigg|_0\Gamma_0^{(1,N)}\,, \tag{35}$$

where, again, the index 0 means differentiation at fixed bare parameters. A new vertex function

$$\Gamma_0^{(1,N)}=\frac{\partial\Gamma_0^N}{\partial m_0^2} \tag{36}$$

appears. This vertex function differs from Γ_0^N by an extra term $\varphi^2(R)$ inside the averaging $\langle\dots\rangle$ in (12). As a result, for the renormalized vertex functions Γ_R^N one obtains an inhomogeneous Callan–Symanzyk equation containing $\Gamma_R^{(1,N)}$ on the right-hand side. However, close to the critical point $m=0$ the right-hand side can be neglected with respect to the left-hand side and one arrives at the homogeneous Callan–Symanzyk equation which repeats the structure of the RG Eqn (19):

$$\bigg(m\,\frac{\partial}{\partial m}+\beta_u\,\frac{\partial}{\partial u}+\beta_v\,\frac{\partial}{\partial v}-\frac{N}{2}\,\gamma_\phi\bigg)\Gamma_R^N(m,u,v)=0\,, \tag{37}$$

where the coefficients β_u, β_u, and γ_ϕ are defined by relations (20)–(22), and the parameter μ here is to be understood as the renormalized mass m. The partial differential equation (37) is solved by the method of characteristics, which is sketched by relations (24)–(26) and leads to the fixed-point relations given by (27)–(31).

For the sake of completeness, let us note that the finiteness of the renormalized vertex function $\Gamma_R^{(1,2)}$ with one ϕ^2 insertion is achieved by the familiar renormalizing factor $\bar{Z}_{\phi^2}$

$$\Gamma_R^{(1,2)}(k;q,-q;m,u,v)=\bar{Z}_{\phi^2}\Gamma_0^{(1,2)}(k;q,-q,m_0,u_0,v_0)\,. \tag{38}$$

Then, formula (30) for the correlation-length critical exponent ν may be recast in terms of $\bar{Z}_{\phi^2}$ by a substitution $2\gamma_m=\gamma_\phi+\bar{\gamma}_{\phi^2}$, which follows from the relations $Z_{m^2}=\bar{Z}_{\phi^2}Z_\phi^{-1}$ and

$\bar{\gamma}_{\phi^2} = \mu\,\partial \ln \bar{Z}^{-1}_{\phi^2}/\partial\mu|_0$. This leads to the relation

$$\frac{1}{\nu} = 2 - \gamma_\phi(u^*, v^*) - \bar{\gamma}_{\phi^2}(u^*, v^*)\,. \tag{39}$$

The explicit expressions for the RG β and γ functions are scheme-dependent: they differ in different renormalization schemes. Consequently, the fixed-point coordinates are scheme-dependent as well. However, the RG functions coincide in different schemes once calculated at the fixed point. This leads to the same asymptotic values of the critical exponents: they are universal and do not depend on the renormalization scheme [108, 109]. In the next subsection, we will give available expansions for the RG functions of RIM.

5.2 Perturbation expansion series and their 'naive' analysis

Expressions for the RG functions of RIM are obtained as series in renormalized couplings u and v. The perturbation theory in powers of u and v is in fact a perturbation theory in the number of integrations in **k** space. On the other hand, this corresponds to the number of loops in Feynman diagrams in the diagrammatic representation for the vertex functions [108]. By now, the RIM RG functions are known up to the order of five loops in the minimal-subtraction scheme [115] and with a record six-loop accuracy when calculated directly for $d = 3$ in the massive scheme [66].

Written in the minimal-subtraction scheme, the functions read

$$\beta_u = -u\left(\varepsilon - u - \frac{3}{2}\,v + \frac{17}{27}\,u^2 + \frac{23}{12}\,uv + \frac{41}{32}\,v^2 + \ldots + \beta_u^{(5LA)}\right), \tag{40}$$

$$\beta_v = -v\left(\varepsilon - v - \frac{2}{3}\,u + \frac{21}{32}\,v^2 + \frac{11}{12}\,vu + \frac{5}{27}\,u^2\right), \tag{41}$$

$$\gamma_\phi = \frac{1}{54}\,u^2 + \frac{1}{24}\,uv + \frac{1}{64}\,v^2 + \ldots + \gamma_\phi^{(5LA)}, \tag{42}$$

$$\bar{\gamma}_{\phi^2} = \frac{1}{3}\,u + \frac{1}{4}\,v - \frac{1}{9}\,u^2 - \frac{1}{4}\,uv - \frac{3}{32}\,v^2 + \ldots + \bar{\gamma}_{\phi^2}^{(5LA)}\,. \tag{43}$$

Here and below, we give the RG functions in the convenient normalization, where the one-loop coefficient at u (v) equals unity in the corresponding function β_u (β_v). We write down the functions only up to the two-loop approximation (2LA), referring to paper [57] where they were obtained in 3LA. Four- and five-loop contributions may be derived from the RG functions of the anisotropic cubic model obtained in Ref. [115].

Note that in the minimal-subtraction scheme the dependence on the space dimension d is trivial and enters into expressions (40)–(43) only via a single term proportional to $\varepsilon = 4 - d$ explicitly written in the β functions (40) and (41). On the contrary, in the massive scheme the space dimension d enters into the expressions for the loop integrals, corresponding to each Feynman diagram of perturbation expansion. Consequently, the theory is evaluated at a space dimension that is of interest. Values of the loop integrals for fixed space dimension $d = 2$ and $d = 3$ are given in [116]. The series for RG functions of the $d = 3$ RIM read

$$\beta_u = -u\left(1 - u - \frac{3}{2}\,v + \frac{308}{729}\,u^2 + \frac{104}{81}\,uv + \frac{185}{216}\,v^2 + \ldots + \beta_u^{(6LA)}\right), \tag{44}$$

$$\beta_v = -v\left(1 - v - \frac{2}{3}\,u + \frac{95}{216}\,v^2 + \frac{50}{81}\,vu + \frac{92}{792}\,u^2 + \ldots + \beta_v^{(6LA)}\right), \tag{45}$$

$$\gamma_\phi = \frac{8}{729}\,u^2 + \frac{2}{81}\,uv + \frac{1}{108}\,v^2 + \ldots + \gamma_\phi^{(6LA)}, \tag{46}$$

$$\bar{\gamma}_{\phi^2} = \frac{1}{3}\,u + \frac{1}{4}\,v - \frac{2}{27}\,u^2 - \frac{1}{6}\,uv - \frac{1}{16}\,v^2 + \ldots + \bar{\gamma}_{\phi^2}^{(6LA)}. \tag{47}$$

Again, we show here only the two-loop functions. In the ε expansion, these functions were first obtained in Ref. [45]. Three-loop terms first reported in Ref. [48] contained some errors, partially corrected in Ref. [49]. Finally, three-loop expressions free of errors were reported in Ref. [53]. Subsequently, four-loop series were obtained in Ref. [54] and only recently five-loop [64] and record six-loop [66] expansions became available. Universal critical-amplitude ratios at $d = 3$ were first obtained in three-loop approximation [117] and are known by now to an accuracy of five loops [118].

As we noted above, the massive RG scheme does not necessarily mean evaluation at $d = 3$. The possibility of applying the scheme in order to get the RIM RG functions at an arbitrary noninteger space dimension was outlined in Ref. [56]. For the two-loop RG functions, we obtain [56]

$$\beta_u = -(4-d)u\left\{1 - u - \frac{3}{2}v + \frac{8}{27}\left[9\left(i_1 - \frac{1}{2}\right) + i_2\right]u^2 + \frac{2}{3}\left[12\left(i_1 - \frac{1}{2}\right) + i_2\right]uv + \frac{1}{4}\left[21\left(i_1 - \frac{1}{2}\right) + i_2\right]v^2\right\}, \tag{48}$$

$$\beta_v = -(4-d)v\left\{1 - v - \frac{2}{3}u + \frac{1}{4}\left[11\left(i_1 - \frac{1}{2}\right) + i_2\right]v^2 + \frac{2}{3}\left[6\left(i_1 - \frac{1}{2}\right) + i_2\right]vu + \frac{8}{27}\left[3\left(i_1 - \frac{1}{2}\right) + i_2\right]u^2\right\},$$

$$\gamma_\phi = -2(4-d)\left\{\left[\frac{2}{27}\,u^2 + \frac{1}{6}\,uv + \frac{1}{16}\,v^2\right]i_2\right\}, \tag{49}$$

$$\bar{\gamma}_{\phi^2} = (4-d)\left\{\frac{1}{3}\,u + \frac{1}{4}\,v - 12\left[\frac{1}{27}\,u^2 + \frac{1}{12}\,uv + \frac{1}{32}\,v^2\right]\left(i_1 - \frac{1}{2}\right)\right\}.$$

The space dimension d enters into expressions (48) and (49) also by the d-dependent two-loop integrals $i_1(d)$ and $i_2(d)$. Their dependence on d is shown in Fig. 8. Evaluating the integrals [118] for $d = 3$ [$i_1(3) = 2/3$, $i_2(3) = -2/27$], we return to the two-loop contributions of expressions (44)–(47). In the next order of perturbation theory for the noninteger d, the RG functions of RIM are derived in Ref. [60], and the values of the corresponding loop integrals are obtained in Ref. [119].

With the series for the RG functions at hand, there are two different ways to proceed in any of the two RG approaches: (40)–(43) or (44)–(47). In this way, one comes to four different schemes of the analysis. Indeed, the minimal-subtraction scheme can be realized by the familiar ε expansion [120] as well as directly at $d = 3$ [121]. Similarly, the

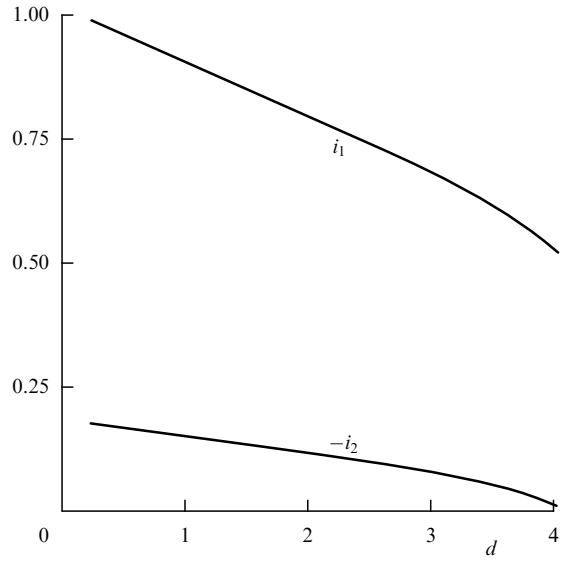

Figure 8. Two-loop integrals of the RG functions in a massive scheme [formulas (48), (49)] as functions of the space dimension d. The figure is taken from Ref. [56].

expressions for the RG functions obtained in the massive scheme can be directly solved for the fixed points or by the pseudo-ε expansion. The latter method was introduced by B G Nickel (unpublished; see Ref. [19] in Ref. [122]). However, as we will see below, only two of these schemes lead to reliable results for RIM critical behavior. Before we proceed, let us discuss this situation in more detail.

1. First, let us consider functions (40)–(43) and perform the ε expansion. In order to obtain the expansion, one should (a) solve the fixed-point equations (27) with ε as a small parameter and (b) substitute the coordinates $u^*(\varepsilon)$ and $v^*(\varepsilon)$ as series in ε into the RG γ-function for the critical exponents.

Looking for fixed-point solutions in a one-loop approximation [i.e., leaving only terms linear in u and v in the brackets in (40) and (41)], one finds three fixed points (compare with Fig. 2): the Gaussian fixed point G, $u^* = v^* = 0$; the pure Ising fixed point I, $u^* \neq 0$, $v^* = 0$ (this describes n noninteracting Ising models, cf. Hamiltonian (8) with $v = 0$); and the 'polymer' fixed point P, $u^* = 0$, $v^* \neq 0$ (putting $u^* = 0$ in (8), we obtain the $O(n = 0)$ model describing the scaling properties of self-avoiding walks). It is straightforward to check that the fixed points G and I are unstable, whereas the fixed point P is stable. However, as far as $v^* > 0$, it is inaccessible for the initial values of couplings of the model under consideration. In a one-loop approximation, the fixed point R with both nonzero coordinates ($u^* \neq 0$ and $v^* \neq 0$) does not exist; this occurs because the system of equations for the fixed points is degenerate on the one-loop level [42, 44, 45]. This fixed point appears in the next (two-loop) approximation, and leads to the qualitative picture shown in Fig. 2. However, because of the degeneracy of the one-loop equations, instead of expanding in ε, one has to expand in $\sqrt{\varepsilon}$ [43, 45]. Proceeding as usual, this leads to $\sqrt{\varepsilon}$ expansions for the critical exponents and the stability matrix (28) eigenvalues [58, 61]:

$$v = 0.5 + 0.08411582\,\varepsilon^{1/2} - 0.01663203\,\varepsilon + 0.04775351\,\varepsilon^{3/2} + 0.27258431\,\varepsilon^2\,, \tag{50}$$

$$\eta = -0.00943396\,\varepsilon + 0.03494350\,\varepsilon^{3/2} - 0.04486498\varepsilon^2 + 0.02157321\,\varepsilon^{5/2}\,, \tag{51}$$

$$\gamma = 1 + 0.16823164\,\varepsilon^{1/2} - 0.02854708\,\varepsilon + 0.07882881\,\varepsilon^{3/2} + 0.56450490\,\varepsilon^2\,, \tag{52}$$

$$\omega_1 = 2\,\varepsilon + 3.704011194\,\varepsilon^{3/2} + 11.30873837\,\varepsilon^2\,, \tag{53}$$

$$\omega_2 = 0.6729265850\,\varepsilon^{1/2} - 1.925509085\,\varepsilon - 0.5725251806\,\varepsilon^{3/2} - 13.93125952\,\varepsilon^2\,. \tag{54}$$

Two-loop expressions for the exponents were obtained in Ref. [45], three-loop results were presented independently in Refs [46] and [47]. The $\sqrt{\varepsilon}$-expansion series for the RIM amplitude ratios [123] are also available to a three-loop accuracy [124]. Due to the five-loop results for an anisotropic cubic model [115], it was possible to obtain four- and five-loop $\sqrt{\varepsilon}$ expansion for the critical exponents [58] (50)–(52) and the stability-matrix eigenvalues [61] (53), (54) of the RIM.

2. The second way of calculation that may be used in the minimal-subtraction RG approach is the $d = 3$ technique [121]. It consists of (a) fixing the value of $\varepsilon = 1$ in (40) and (41), (b) solving the system of fixed-point equations (27) numerically, and (c) substituting the numerical values of the fixed-point coordinates into the series for the critical exponents. The RIM β functions are shown in Fig. 9 in two-loop approximation. One can see that they do not possess nontrivial fixed points at all. However, such behavior is not surprising and is not a particular feature of the RIM. It is well

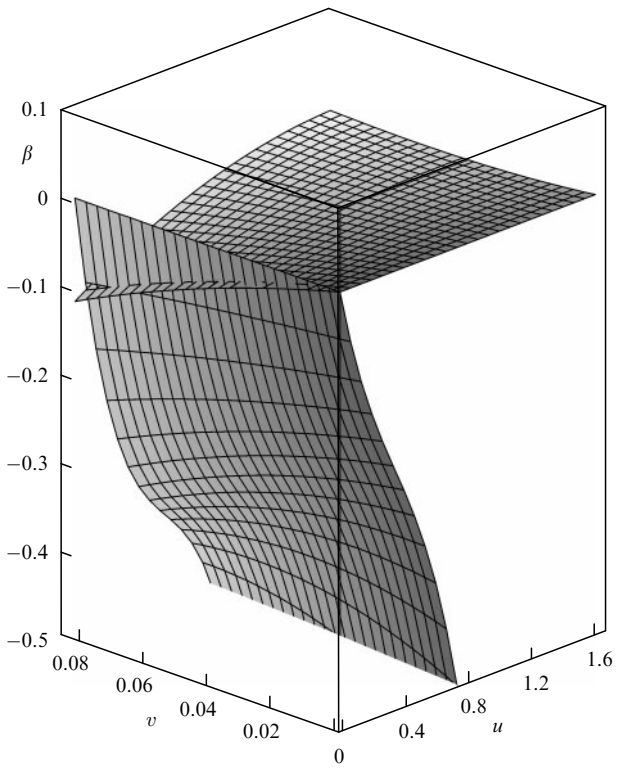

Figure 9. β functions of RIM, $\beta_u(u, v)$ and $\beta_v(u, v)$, calculated in two-loop approximation within a $d = 3$ minimal-subtraction scheme without resummation. Only the Gaussian fixed point $u^* = v^* = 0$ survives. The figure is taken from Ref. [126].

known that perturbation series for the RG functions in the weak coupling limit are asymptotic at best and should be evaluated by means of special resummation techniques. These will be the subject of the next Section 6. Here, to complete the list of possible calculation schemes, we mention two more schemes in the massive RG approach.

3. The massive RG scheme is implemented by (a) numerically solving the system of fixed-point equations (27) and then (b) substituting the numerical values of the fixed-point coordinates into the series for the critical exponents. It is this way that is concerned with in most papers devoted to the RIM RG analysis (see Section 6 for details).

4. The massive RG scheme is also implemented by a pseudo-ε expansion [122, 125]. This scheme is based on the observation that in order to analyze the series (44)–(47) one can imitate an ε expansion by introducing an auxiliary parameter τ instead of the zeroth-order term 1 in the massive-scheme β functions (44) and (45). Then, the fixed-point and critical exponents are obtained as series in τ; to obtain their final values, one puts $\tau = 1$. The described pseudo-ε expansion allows us to avoid cumulation of the errors for the critical exponents from the errors of the fixed-point coordinates and the γ functions. It proved to be highly efficient for the pure $d = 3$ Ising model [73, 122]. For the same reasons that the ε expansion in the case of RIM turns into the $\sqrt{\varepsilon}$ expansion, the expansion in τ turns into a $\sqrt{\tau}$ expansion. On the basis of the six-loop expansions (44)–(47), we obtain the following $\sqrt{\tau}$ expansion for the RIM critical exponents and the stability matrix eigenvalues:

$$\nu = 0.5 + 0.10291260\,\tau^{1/2} + 0.01251853\,\tau + 0.01270178\,\tau^{3/2} + 0.05663757\,\tau^2 + 0.03694322\,\tau^{5/2}, \tag{55}$$

$$\eta = -0.00836820\,\tau + 0.02173733\,\tau^{3/2} - 0.01487714\,\tau^2 + 0.01733771\,\tau^{5/2}, \tag{56}$$

$$\gamma = 1 + 0.20582521\,\tau^{1/2} + 0.02922117\,\tau + 0.01539608\,\tau^{3/2} + 0.11858141\,\tau^2 + 0.06658280\,\tau^{5/2}, \tag{57}$$

$$\omega_1 = 2\,\tau + 2.59761132\,\tau^{3/2} + 7.51800557\,\tau^2 + 39.86825804\,\tau^{5/2}, \tag{58}$$

$$\omega_2 = 0.82330084\,\tau^{1/2} - 1.74713206\,\tau - 1.26569350\,\tau^{3/2} - 8.75074159\,\tau^2 - 40.98838378\,\tau^{5/2}.$$

These expressions should be compared with formulas (50)–(54).

6. Series resummation and numerical results

6.1 Summability of RIM divergent series

The core of the perturbation approach is a sequential account of corrections in expansions in a small parameter. However, such an approach does not necessarily lead to cumulation of the calculation accuracy by a 'naive' summation of successive perturbation-theory terms. It is well known by now that the weak-coupling expansion series for RG functions have zero radii of convergence and are asymptotic at best [109]. Appropriate resummation procedures are to be applied in order to handle them. Early studies of critical phenomena by the ε-expansion technique lead to a concept of an 'optimal truncation' of a series as a maximal number of terms possessing convergent behavior. Such behavior is typical for an asymptotic series [127], where series expansion coefficients grow factorially. For example, the expansion of an RG function $f(u)$ of a pure Ising model in powers of a single renormalized coupling u

$$f(u) = \sum_k A_k u^k \tag{59}$$

was shown to possess the following behavior:

$$A_k = c k^{b_0} (-a)^k k! \left[1 + O\left(\frac{1}{k}\right)\right], \qquad k \to \infty, \tag{60}$$

with known values [128–131] of constants c, b_0, and a. The property (60) indicates the Borel summability of the series (59). The Borel resummation procedure takes into account the asymptotic behavior of the coefficients (60) and maps the asymptotic series (59) to a convergent one with the same asymptotic limit. We will describe the procedure in detail in Sections 6.2 and 6.3.

It is worthwhile to note that a proof of the Borel summability for the ε expansion of a pure Ising model does not exist. Only an expansion in coupling (59) is proved to posses this property [128]. Nonetheless, the rich number of numerical estimates obtained on the basis of the resummed ε expansion for the pure Ising model (see, e.g., [109]) convinces one of its reliability. However, this is not the case for the $\sqrt{\varepsilon}$ expansion of RIM. The fact that ε expansion will not be able to give information on critical exponents in a system with quenched disorder was predicted already in Refs [132, 133] by studying the randomly diluted model in zero dimensions. The perturbation-theory series of this 'toy' model appeared to be Borel-nonsummable. Moreover, such properties were shown [133] to be a direct consequence of the existence of Griffiths-like singularities [79] caused by the zeroes of the partition function of the pure system. Although the $\sqrt{\varepsilon}$ expansion allowed one to predict a qualitatively new critical behavior of the RIM [43, 45], it seems to be of no use for a quantitative analysis. Moreover, by naively adding the successive perturbational contributions in the $\sqrt{\varepsilon}$ expansion for the RIM stability-matrix eigenvalues (53) and (54), one already observes that in the three-loop approximation ($\sim \varepsilon$) ω_2 becomes negative and, therefore, no stable fixed point exists in a strict $\sqrt{\varepsilon}$ expansion [61]. Even the resummation procedures applied do not change this picture [63]. Quite different convergence properties of the expansions for a pure $d = 3$ Ising model and RIM may already be seen by applying a simple Padé analysis, as was shown in Refs [59, 63].

The above-mentioned divergent properties of the $\sqrt{\varepsilon}$ expansion concern also the pseudo-$\sqrt{\varepsilon}$ expansion (55)–(58) derived in Section 5. So, there remain only two out of four different ways of numerical analysis of the RIM RG functions. They are denoted by 2 and 3 in the preceding Section 5.2. Both are based on analysis of RG series in two couplings. The nature of the RIM RG function expansions in couplings u and v remains open for discussion. Nonetheless, the resummation procedures that in different modifications are used in the analysis of asymptotic series have been applied fruitfully to the RIM RG series as well [51–57, 59–

65]. The method which prevails in the resummation of the RIM RG series is the generalization of the Padé – Borel resummation technique [134] for the case of two variables. We will review the results based on such a resummation in the next Section 6.2.

Recently, it was shown that the expansions for the quenched diluted Ising model in $d = 0$ dimensions are Borel-summable, provided a specific means of summation is applied [135]. This allowed the authors of Ref. [65] both to recover the asymptotic behavior of the expansion coefficient and to apply the resummation technique refined by conformal mapping to RIM six-loop massive RG functions [66]. This method will be reviewed in the last Section 6.3.

6.2 Padé – Borel oriented resummation

In order to perform the Padé – Borel resummation of a truncated (asymptotic) series in a single variable (e.g., series (59) with L terms available), one defines the Borel – Leroy image of the initial sum $S = \sum_{i=0}^{L} a_i u^i$ by

$$S^{\mathrm{B}}(u) = \sum_{i=0}^{L} \frac{a_i u^i}{\Gamma(i+q+1)}\,, \tag{61}$$

where $\Gamma(x)$ is Euler's gamma function and q is an arbitrary nonnegative number, which will serve as a fit parameter. The result (61) is extrapolated by means of a rational approximant $[M/N](u)$, which is the quotient of two polynomials in u with M as the order of the numerator and N as that of the denominator (a Padé approximant [136]). Finally, the resummed function S^{res} is obtained in the form

$$S^{\mathrm{res}}(u) = \int_0^\infty \mathrm{d}t\, \exp(-t) t^q \Big[M/N\Big](ut)\,. \tag{62}$$

In the analysis of single-variable RG functions, this procedure was initiated in Refs [134].

There are different ways to generalize single-variable Padé approximants for the case of two variables (u, v) [136] and, accordingly, to generalize the resummation procedure (61) and (62). One possibility is to construct a series in a single dummy variable x (the so-called resolvent series [137]). The variable is introduced by a substitution $u \to ux$, $v \to vx$, and x must be put equal to 1 to obtain the final results. Accordingly, the Borel – Leroy image of a truncated series $S = \sum_{0 \leqslant i+j \leqslant L} a_{i,j} u^i v^j$ is defined by

$$S^{\mathrm{B}}(x) = \sum_{0 \leqslant i+j \leqslant L} \frac{a_{i,j} (ux)^i (vx)^j}{\Gamma(i+j+q+1)}\,. \tag{63}$$

Then, the series in x is resummed by formula (62) and evaluated at $x = 1$. We will refer to this method below as the Padé – Borel method, similar to the one-coupling case.

Another way to proceed is to make use of the Chisholm approximants [136, 138] which are the generalization of Padé approximants to the many-variable case. A Chisholm approximant can be defined as a ratio of two polynomials both in variables u and v, of degree M and N such that the first terms of its expansion are equal to those of the function that is approximated. Again, the resummation is performed by Eqn (62), however, with the Chisholm approximant instead of the Padé approximant. This method will be referred to below as the Chisholm – Borel resummation.

For a given Borel – Leroy image, many approximants, both Padé and Chisholm, can be constructed. However, restrictions are imposed naturally. First, an approximant should be chosen in the form re-constituting the sign-alternating high-order behavior of the general term of β and γ functions [66]. The approximant generating a sign-alternating series might be chosen in a form $[M/1]$ with the positive coefficients at the variable x (or u and v). However, it is the diagonal approximants that give the best convergence in the Padé analysis [136] (see also [63] for a toy model example). On the other hand, a high degree of a polynomial in the denominator often leads to poles on the positive semiaxis. One can use analytic continuation and calculate the principal value of integral (62) to process the singularities; however, practical calculations force us to reject this generalization. The reason is both the unexpected shift of fixed-point location and the different topological structure of the lines of zeroes for the resummed β functions. The choice of a Chisholm approximant is even more complicated, since often its coefficients are undetermined. For instance, the construction of a nontrivial approximant for a two-variable polynomial of a second order requires two additional conditions to be imposed. Normally they are chosen to preserve certain symmetry properties. Provided the couplings u_0 and v_0 enter into the Hamiltonian (8) symmetrically, the approximants must be symmetric in variables u and v in order not to introduce an additional symmetry. Another point is that by substitution $v = 0$ all the equations that describe the critical behavior of the diluted model are converted into appropriate equations of the pure model. However, if the pure model is considered independently, the resummation technique with the application of the Padé approximant is used. Thus, the Chisholm approximant is to be chosen in such a way that, by putting any u or v equal to zero, one reproduces familiar results for the one-variable case. This also implies a special choice of additional conditions.

Most numerical results on the universal characteristics of RIM at criticality were obtained on the basis of the massive renormalization scheme by numerically solving fixed-point equations (27) for the resummed β functions (44) and (45) and resumming the γ functions (46) and (47) in the stable fixed point (scheme 3 in Section 5.2). The study of the massive β functions of RIM resummed in this way revealed that, starting from the two-loop approximation, the random fixed point (R in Fig. 2) is stable and is present in all orders of perturbation theory [51 – 56, 60, 62, 64, 139]. As an example, in Figs 10 and 11 we show the lines of zeroes of functions $\beta_u(u, v)$ and $\beta_v(u, v)$ in different orders of perturbation theory without resummation and resummed by the Chisholm – Borel method. One can see that without resummation all nontrivial fixed points are obtained only in the three-loop approximation. Resummation restores the presence of nontrivial fixed points.

The massive scheme of the field-theoretical renormalization group was the basis of the first numerical estimates of RIM critical exponents. Alternatively, the nonperturbative scaling-field approach for solution of the Wilson's renormalization-group equation was used to study RIM critical behavior in Ref. [50]. This approach, similarly to ε expansion, permits us to treat the model in continuous dimensions d. As a result, RIM critical exponents were found for $2.8 \leqslant d \leqslant 4$. The scaling-field approach was not followed by more precise calculations.

Already the study of two-loop RIM massive RG functions resummed by the Chisholm – Borel procedure [51] revealed that no difficulties connected to the degeneracy of the β functions are encountered. Critical exponents extracted

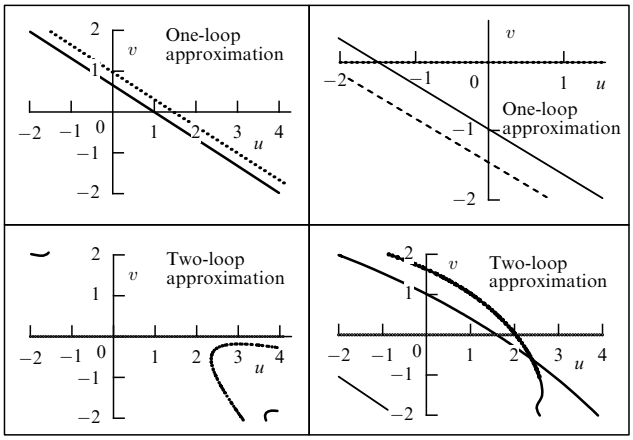

Figure 10. The lines of zeroes of nonresummed (left-hand column) and resummed by the Chisholm – Borel method (right-hand column) RIM massive β functions in different orders of the perturbation theory: one- and two-loop approximations. Circles correspond to $\beta_u = 0$, thick lines depict $\beta_v = 0$. Thin solid and dashed lines show zeroes of the analytically continued functions β_u and β_v respectively. One can see the appearance of a mixed fixed point $u > 0$, $v < 0$ in the two–loop approximation for the resummed β functions. The figure is taken from Ref. [60].

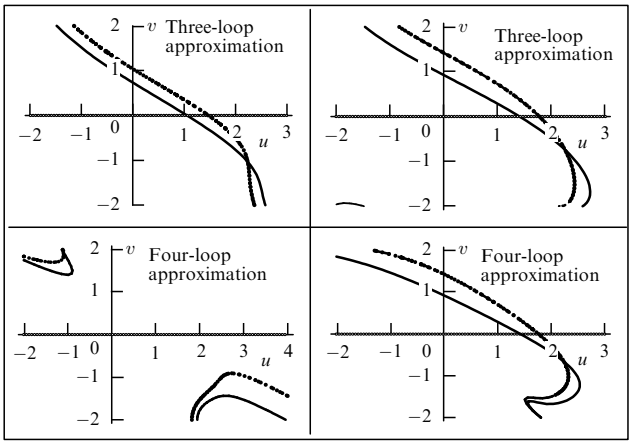

Figure 11. The lines of zeroes of nonresummed (left-hand column) and resummed by the Chisholm – Borel method (right-hand column) RIM massive β functions in different orders of the perturbation theory: three- and four-loop approximations. The notations are the same as in Fig. 10. In the vicinity of the mixed fixed point the behavior of the resummed functions remains alike with an increase of the order of approximation. This is not the case for the nonresummed functions. The figure is taken from Ref. [60].

from resummed γ-function values at the fixed point were found to be clearly larger than the pure-model ones (see Table 3). As noted above, in the three-loop level the straightforward analysis of the β functions [48, 49] yielded fixed-point coordinates and critical exponents without resummation, but the accuracy obtained did not allow us to estimate, for instance, heat capacity critical behavior. On the other hand, the application of the Padé – Borel technique also encountered hardships within the three-loop level (see diagram in Fig. 12). Here, the approximant with a linear denominator does not yield a fixed point, while another near-diagonal approximant $[1/2]$ is unreliable because it reveals a fixed point only when calculating the principal value of the corresponding integral via analytic continuation. When treated by means of a Chisholm – Borel technique, the same expressions allowed one to obtain asymptotic critical exponents of RIM [52, 53].

The four-loop results [54] were resummed by means of the Chisholm – Borel [54], the first confluent form of the ϵ algorithm of Wynn [55], and the Padé – Borel [55, 62] methods and showed close results (see Table 3 and diagram in Fig. 12). Whereas Padé – Borel calculations of Ref. [55] exploited the [3/1] Padé approximant, Ref. [62] used a more elaborated generalized Padé – Borel – Leroy resummation method. The last is based on exploiting all possible Padé approximants in the Borel – Leroy resummation (61) – (62), choosing for each of them the optimal value of the Leroy parameter q and then averaging the result over all values given by the approximants [62].

The analysis of expressions in the five-loop approximation with the application of the fit parameter q required rather artificial rejection of many approximants [64]. For instance, using a criterion that it is those approximants are working that provide maximal stability against variation of q, the approximant $[2/2]$ was chosen to estimate u^* and the approximant $[3/1]$ to obtain v^*. The analysis allowed the authors of Refs [64] to obtain five-loop estimates for the RIM critical exponents (see Table 3). However, the extension to the six-loop order revealed a wide gap between five- and six-loop fixed-point coordinates [139] with respective inconsistency in the six-loop values of critical exponents compared with the five-loop results of Refs [64]. This might serve as indirect evidence of the possible nonasymptotic nature of the series under consideration.

A similar resummation technique was also applied to the minimal-subtraction RG functions (40) – (43) directly at $d = 3$ (scheme 2 in Section 5.2) [57, 59, 61, 63]. Here, asymptotic behavior, as well as effective critical behavior, was studied. Again, as in the massive RG case, resummation restores the presence of the nontrivial fixed point in the two-loop approximation (see Fig. 13) and preserves it in three- [57] and four-loop approximations [59, 63]. However, in the five-loop order the applied Chisholm – Borel resummation scheme did not lead to a real root for the random fixed point [59, 63]. One of reasons for such behavior may be possible Borel-nonsummability of the series under consideration. In this case the four-loop approximation will be an 'optimal truncation' for the resummed minimal-subtraction perturbation-theory series, similar to the nonresummed asymptotic series. It is known for the ε expansion of the $O(n)$-symmetric ϕ^4 model that a 'naive' interpretation of the series truncated by the ε^2 term leads to the best (optimal) result.

Values of asymptotic critical exponents obtained in three- [57] and four- [59, 61, 63] loop approximations are listed in Table 3; effective exponents were calculated [57, 63] by resummation of formulas (34). Figure 14 shows the solutions $u(l)$, $v(l)$ of the flow equations (25) calculated by the Chisholm – Borel resummation of four-loop β functions (40), (41) [63]. The flows shown in Fig. 14 predict several different scenarios for the behavior of the effective critical exponents (see Figs 15, 16). Both in experiment and in computer simulations (see Tables 1, 2), the exponents reported differ from and even exceed the known asymptotic theoretical values. This nonuniversal behavior might be related to the possible nonasymptotic behavior found in different flows, as has been suggested in Refs [30, 57]. The difference might be due to (a) the different temperature

Table 3. The theoretical values of asymptotic critical exponents of RIM. *

References	RG scheme	Order	Summation	ν	η	γ	ω
Sokolov et al., 1981 [49]	massive	3LA	No		0.009	1.31	
Newman et al., 1982 [50]	SF	No		0.70	0.015	1.39	0.41
Jug, 1983 [51]	massive	2LA	ChBr	0.678	0.031	1.336	0.450^{c}
Mayer et al., 1984 [52]	massive	2LA 3LA	ChBr ChBr		0.031 0.022	1.337 1.325	
Mayer et al., 1989 [54]	massive	4LA	ChBr	0.670	0.034	1.326	
Mayer, 1989 [55]	massive	4LA 4LA	AW PdBr	0.6680 0.6714		1.318 1.321	
Shpot, 1989 [53]	massive	3LA	ChBr	0.671	0.021	1.328	0.359
Janssen et al., 1995 [57]	MS, $d = 3$	3LA	PdBr	0.666		1.313	0.366
Holovatch et al., 1997 [60]	massive	3LA	ChBr	0.671	0.019	1.328	0.376
Folk et al., 1998 [59]	MS, $d = 3$	2LA 3LA 4LA	ChBr	0.665 0.654 0.675	0.032 0.022 0.049	1.308 1.293 1.318	0.162 0.430 0.390^{c}
Folk et al., 1999 [61]	MS, $d = 3$ massive	4LA 4LA	ChBr ChBr				0.39(4)^{c} 0.372(5)
Pakhnin et al., 2000 [64]	massive	5LA	PdBr	0.671(5)	0.025(10)	1.325(3)	0.32(6)
Varnashev, 2000 [62]	massive	4LA	PdBr PdBr	0.681(12) 0.672(4)	0.040(11) 0.034(10)	1.336(20) 1.323(10)	 0.330
Pelissetto et al., 2000 [65]	massive	6LA	PdBr – CM PdBr – PdBr	0.678(10) 0.668(6)	0.030(3) 0.0327(19)	1.330(17) 1.313(14)	0.25(10) 0.25(10)

* nLA denotes the nth order in loopwise approximation within massive ('massive') and $d = 3$ minimal-subtraction ('MS') schemes of the field-theoretical renormalization-group approach. The resummation procedures are given in the following notations: ChBr, Chisholm – Borel; PdBr, Padé – Borel; AW, ε-algorithm of Wynn; and CM, Borel transformation with conformal mapping. SF stands for the Golner – Riedel scaling-field approach, and superscript 'c' at the correction-to-scaling exponent ω indicates that the real part of the corresponding complex number is shown.

regions of the experiment and/or (b) the different concentrations. The initial values for the couplings in the flow equations depend on the value of the concentration; in particular, for a small dilution one expects the coupling v to be proportional to the concentration. If this is the case, one expects a monotonic increase in the values of the effective exponent to the asymptotic value. A typical scenario is presented by curves *3* in Figs 14 – 16. In this case effective exponents equal to the pure model critical exponents might be found in a relatively wide region of temperature. Then, as the attraction region of the fixed point *I* becomes weaker and weaker, overshooting is possible, where effective exponents larger than their asymptotic values might be found. This scenario is predicted for larger dilutions and represented by curves *6* in Figs 14 – 16. Curves *4* and *5* correspond to the situation where crossover from the mean-field behavior toward the random one is not influenced by the presence of a pure fixed point *I*.

6.3 Resummation based on conformal mapping

The resummation procedure based on conformal mapping is widely used in the analysis of asymptotic series for models with one coupling, in particular for the pure $d = 3$ Ising model (scalar ϕ^4 theory, see, e.g., [73, 109, 122]). However, an application of such a method assumes that the behavior of high-order terms of the series is known. It is not the case for RIM. This explains why in the studies of RIM the Padé – Borel-based resummation technique was used, as described in Section 6.2. However, by studying the $d = 0$ quenched diluted Ising model, it was recently shown analytically [135] that the perturbative expansions for the free energy are Borel-summable, provided the summation is carried out in a special way. The main results of Ref. [135] state that if the double expansion of the RIM functions in powers of u and v is written as

$$f(u, v) = \sum_{i=0}^{\infty} c_i(v) u^i , \tag{64}$$

$$c_i(v) = \sum_{j=0}^{\infty} c_{ij} v^j , \tag{65}$$

then expansion (65), as well as expansion (64) at fixed v is Borel-summable. These results enabled the authors of Ref. [65] to perform the resummation of the six-loop series (44) – (47) (see [66]). Moreover, by noticing that the large-order behavior of the series (65) can be derived on the basis of

	0	1	2	3	4	5	6
0	–	–	–	–	–	–	–
1	–		±	–	–	–	
2	–	–	[62]	∼	∼		
3	[48, 49]	[55, 62]	[64]	∼			
4	–	[64]	±		Approximant		
5	–	∼			not determined		
6	–						

Figure 12. The effectiveness of Padé – Borel resummation for the RIM β functions in a massive scheme. The order numbers of a row M and of a column N correspond to a Padé approximant $[M/N]$ representing a $(M+N)$-loop approximation. The symbol '–' denotes that no fixed point can be obtained on the base of a given approximant; '±' and '∼' indicate either the implementation of the analytic continuation (due to poles on the real semiaxis) or a situation where coordinates of the obtained fixed point are far from their expected values. The fruitful approximants are shown by shading and/or appropriate citations. Though working approximants are distributed rather stochastically, the numerical results based on them show evident convergence (see Table 3).

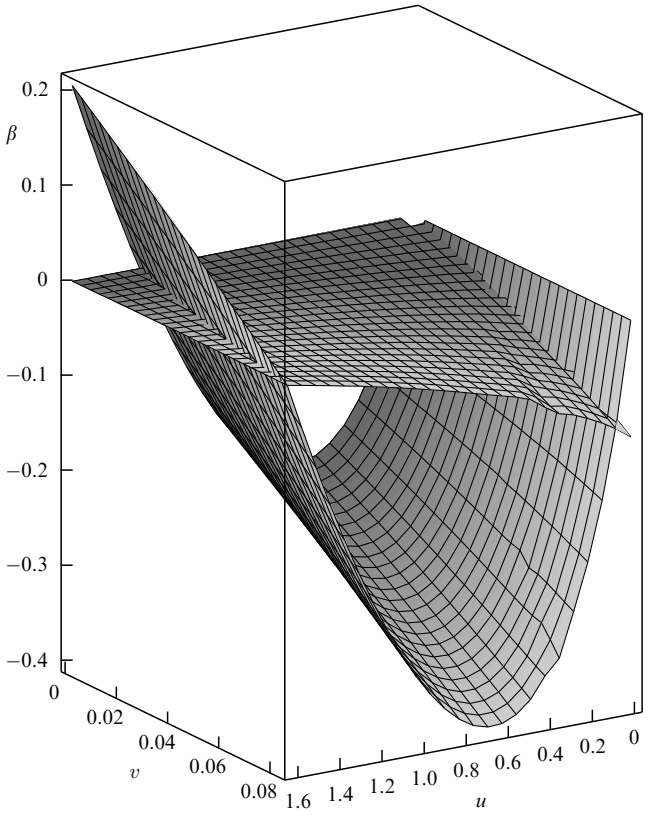

Figure 13. Application of the Padé – Borel resummation technique to the β functions of Fig. 9. Resummation restores the fixed point $u^* \neq 0$, $v^* = 0$ and permits one to obtain a new stable fixed point $u^* \neq 0$, $v^* \neq 0$. The figure is taken from Ref. [126]. (Note that the authors of Ref. [129] exploited a different normalization of couplings, $u \to 3/2\,u$ and $v \to -4\,v$, in comparison to formulas (40) – (43).)

known asymptotics (60) (see [129 – 131]), they were able to perform the resummation based on conformal mapping for the series in v (65) to get convergent results for the coefficients $c_i(v)$.

The procedure of conformal-mapping resummation of a series in a single variable u is standard [122, 140]. For a given Borel – Leroy transform $S^{\mathrm{B}}(u)$ (61), the initial series may be restored from

$$S^{\mathrm{res}}(u) = \int_0^\infty \mathrm{d}t\, \exp(-t)\, t^b\, S^{\mathrm{B}}(ut)\,. \tag{66}$$

Assuming the asymptotic behavior of the general term in the form (60), one concludes that the singularity of the transformed series $S^{\mathrm{B}}(u)$ closest to the origin is located at the point $(-1/a)$. Conformally mapping the cut plane u onto a unit disk and leaving the origin invariant (see Fig. 17),

$$w = \frac{(1+au)^{1/2}-1}{(1+au)^{1/2}+1}, \qquad u = \frac{4}{a}\,\frac{w}{(1-w)^2}\,, \tag{67}$$

substituting the result into $S^{\mathrm{B}}(u)$, and reexpanding in w, one receives a series defined on disk with radius 1 in the w plane. This series is then resubstituted into Eqn (66). In order to weaken a possible singularity in the w plane, the corresponding expression is multiplied by $(1-w)^\rho$ and, thus, one more parameter, ρ, is introduced [140].

However, the above procedure may be applied only to the RIM RG series for the coefficients c_i (65), inasmuch as the large-order behavior (60) may be derived only for series in v (65) (see [65]). The asymptotics of the resulting series in u (64) is still unknown. This compels one to apply the Padé – Borel resummation technique for their analysis. It can be applied to series (65) as well. In summary, this leads to different ways of series resummation: (i) applying the Padé – Borel method both for series (64) and (65) (in Ref. [65] this technique is called the 'double Padé – Borel method') and (ii) applying the conformal method for series (65) and the Padé – Borel method for series (64) ('conformal Padé – Borel method'). Both approaches were implemented in Ref. [65], paying special attention to the choice of different Padé approximants as well as optimizing the results on the basis of fit parameters. In Table 3 we display the data for the RIM critical exponents proposed by the authors on the basis of the analysis of the six-loop RG functions, containing estimates on the basis of both the double Padé – Borel method and the conformal Padé – Borel method (we denote them as PdBr – CM). Separately, we give the results of the analysis by the double Padé – Borel method (PdBr – PdBr). Let us note that the conformal-mapping technique appears to give more robust results, even in resumming the RG series for fixed v^*/u^*. Applying a procedure of conformal-mapping-based resummation of Ref. [66], the authors of Ref. [65] obtained for the six-loop RG series values of critical exponents which are in quite good agreement with the other estimates (see Table 3). However, the estimates of the fixed-point coordinates differ essentially in different calculation schemes. This leads us to the conclusion [65] that probably the optimal truncation of the RIM β functions corresponds to a shorter series than a six-loop one.

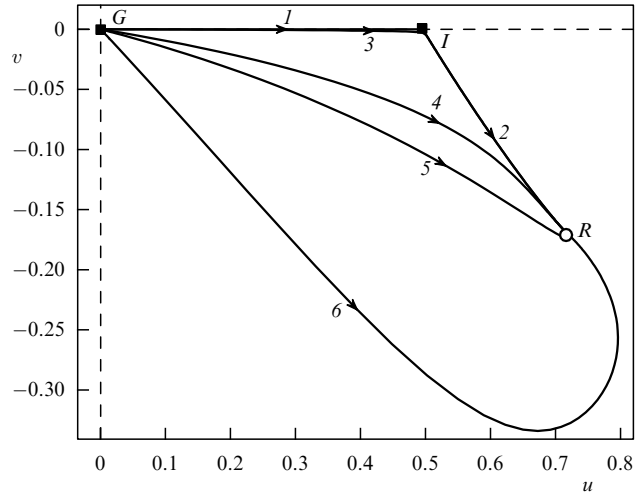

Figure 14. Flow lines for the RIM. Fixed points G and I are unstable, fixed point R is stable. The figure is taken from Ref. [63]. (Note that the authors of Ref. [63] exploited a different normalization of couplings, $u \to 3u$ and $v \to 8/3\,v$, in comparison to formulas (40)–(43).)

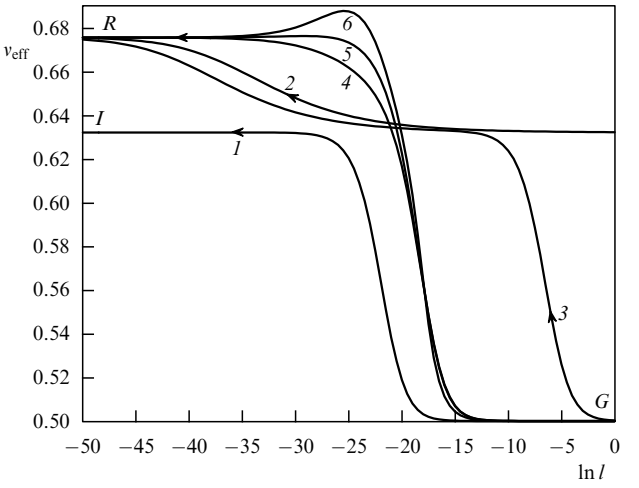

Figure 15. Effective exponent ν_{eff} as a function of the logarithm of the flow parameter ℓ for the flows shown in Fig. 14. The figure is taken from Ref. [63].

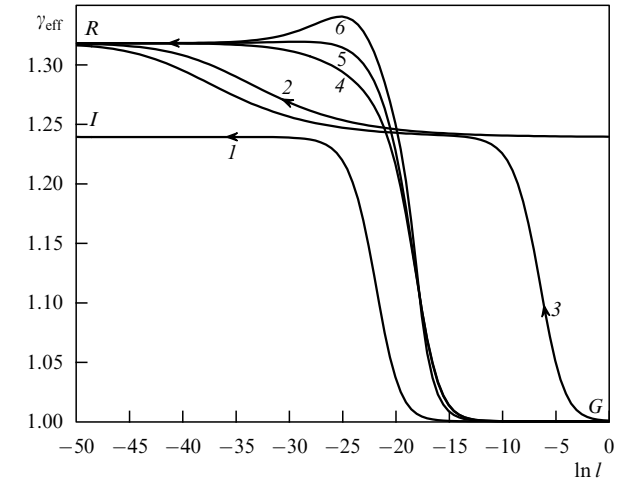

Figure 16. Effective exponent γ_{eff} as a function of the logarithm of the flow parameter ℓ for the flows shown in Fig. 14. The figure is taken from Ref. [63].

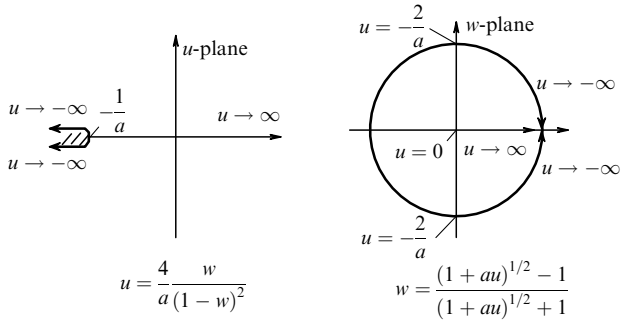

Figure 17. Conformal mapping of a plane with a cut along the negative semiaxis onto a unit disc. The origin remains unchanged in accordance with formulas (67). See the main text for details. The figure is taken from Ref. [141].

7. Conclusion

In this article, we have reviewed results obtained so far in the description of critical properties of a three-dimensional weakly diluted quenched Ising model (RIM). Following the prevailing bulk of experimental, Monte Carlo, and theoretical studies, we focused our attention on the critical exponents of the model. The large number of papers devoted to the precise determination of the exponents undoubtedly bears witnesses to the great interest in the problem. The reason for this is twofold: (i) at the level of a simple model, RIM allows us to include into consideration macroscopic effects of disorder always present in real substances; and (ii) the study of the influence of disorder on universal properties of critical behavior, aside from practical needs, is of high academic interest. It is precisely the domain very close to critical temperature where even a very small amount of impurities can change the properties drastically in comparison with an ideal magnet. In accordance with the heuristic Harris criterion [71], only when the specific heat of an ideal system is divergent at criticality, the disordered magnet is characterized by new critical exponents. The change in critical exponents of RIM is well established both in experimental and Monte Carlo and theoretical studies. However, the numerical values obtained show much worse self-consistency as compared to the situation in studies of pure Ising magnets. This happens due to both technical and principal difficulties. Moreover, often the technical difficulties in determining the RIM exponents are caused by the principal ones.

Though it is commonly believed that various defects are inevitable in experimental samples, the number of experimental RIM studies is much fewer than those devoted to the determination of the Ising-model critical exponents. As an explanation, one might mention that the Ising-model universality class includes not only magnets but also simple fluids, ferroelectrics, binary alloys, etc. Moreover, the RIM itself can show an effective critical behavior of the same type as that in the Ising-model universality class. The data for experimentally determined RIM critical exponents are collected in Table 1. As a peculiarity we note that already in early studies [4] a difference between the critical behavior of RIM and the pure Ising model was observed. Surprisingly enough, since that work neither the experimental precision of the determination of the critical exponents has increased nor could a narrower temperature interval around the critical point be accessed. This can be explained by noting that

starting from the end of the eighties the researchers' attention shifted to the random-field Ising model and the data for RIM were obtained only as side-product results. It is worthwhile to note that the theoretically predicted critical exponents for quenched disorder [65] ($\nu \simeq 0.678$, $\gamma \simeq 1.330$) and for annealed disorder[4] ($\nu \simeq 0.708$, $\gamma \simeq 1.391$) are different, but only slightly. Most probably, one can suggest a scenario according to which in real samples one observes an intermediate situation, and then an exact coincidence between experiments on diluted crystalline antiferromagnets and theoretical calculations can hardly be expected.

While the existence of a new universality class for the RIM has been observed already in early experimental studies, this was not the case in Monte Carlo simulations. Due to the lack of a proper finite-size analysis, a continuous dependence of the critical exponents on concentration was observed. The exponents were interpreted as effective critical exponents [68, 69]. Subsequently, it was crucial to recognize the role of the correction-to-scaling exponent in the analysis of the simulation data [33–35]. This allowed one to conclude from the numerical data the concentration-independent asymptotic critical exponents [33]. As one can note from Table 2, the improvement of computers, as well as of the calculation algorithms, has allowed one to increase the accuracy of critical exponents. Recently, in Monte Carlo simulations of RIM, attention was paid also to the study of the problems of self-averaging in diluted systems [37, 38].

The results of experimental studies and Monte Carlo simulations are confirmed by theoretical calculations. The numerical values of critical exponents obtained by different theoretical methods are collected in Table 3. Note that all theoretical results were obtained within the renormalization-group approach, and most of them within its field-theoretical formalism on the basis of the effective Landau–Ginzburg–Wilson Hamiltonian (8). Though the last approach encounters intrinsic difficulties (such as problems with the breakdown of replica symmetry and the possible existence of a Griffiths phase [79]), it remains the only method which allows one to calculate the asymptotic values of exponents. For the pure Ising model, many results are also based on other methods, in particular, on high- and low-temperature expansions.

Another evident difference of RIM in comparison with the Ising model lies in the applicability of certain computation schemes within the field-theoretical renormalization-group approach, and the failure of others. In the case of the pure Ising model, both massive and minimal-subtraction schemes followed by ε expansion provide consistent and reliable results. For RIM, the ε expansion degenerates into $\sqrt{\varepsilon}$ expansion [43, 45, 58, 61], which appeared to be of no use for quantitative studies [59, 63]. Moreover, the initial series in couplings, both in the massive and the minimal-subtraction schemes, seem not to be Borel-summable [132, 133, 135]. Nevertheless, Padé–Borel-like resummation procedures were employed and allowed one to obtain convergent sequences for the critical exponents within low orders of perturbation theory. This is evident from the agreement of the theoretical results obtained in different orders of perturbation theory (Table 3) with the data of experimental (Table 1) and Monte Carlo (Table 2) studies. However, the resummation failed in higher orders, which resulted in the conjecture that there exists an optimal truncation for the RIM RG functions [63].

On the basis of the six-loop RG functions of the massive scheme, results could only be obtained [65] by means of a highly sophisticated resummation procedure [135]. In the framework of this scheme, the estimates for critical exponents are characterized by the same order of accuracy as for the Ising model, which are based [73] on six-loop expansions for RG β functions and seven-loop expansions for γ functions. However, the determination of error-bars in the theoretical calculations is a difficult problem which is solved in various ways [62, 65]. Here, the errors seem to measure the uncertainty of specific theoretical procedures rather than the confidence intervals of true values.

For a comparison of the theoretical predictions with experimental and simulation data, one should use effective critical exponents, which have been calculated for the RIM within the RG approach [57, 63].

At the very end of this review we want to attract attention again to the fact that the new critical behavior corresponding to the RIM universality class was experimentally observed so far only in magnetic systems like (anti)ferromagnets (see Table 1). Still, it remains a challenge to set up an experiment showing RIM behavior in other condensed-matter systems. A promising example might be a fluid near its liquid–gas critical point in a porous medium. One should note that only in a special case are liquids in porous media an example of the site-diluted Ising model; otherwise, they are conjectured to be examples for random-field models (see for instance [142]). Recently, precise experiments on the critical behavior of liquid helium-4 near the superfluid transition in porous medium [143] confirmed the irrelevancy of quenched disorder. This was expected from the Harris criterion, since the specific heat exponent near the superfluid transition is equal to $\alpha = -0.01056 \pm 0.00038$ [144], which is less than zero within error bars. Thus, an experimental study of a simple liquid in a porous medium may provide the first observation of critical RIM behavior in a nonmagnetic system.

Acknowledgments. In writing this review and carrying out studies of RIM, we benefited from discussions and contacts with numerous colleagues. We greatly acknowledge useful discussions with David Belanger, Bertrand Berche, Christian von Ferber, Hagen Kleinert, Victor Martín-Mayor, Alan McKane, Verena Schulte-Frohlinde, Mykola Shpot, and Aleksandr Sokolov. The materials presented here were used in part during lectures given by one of us in the summer semester 2001 at the Université Henri Poincaré, Nancy 1 (France). Yu H expresses his thanks to Bertrand Berche and colleagues at the Laboratoire de physique des matériaux (Université Nancy 1) for their hospitality, support, and many useful comments.

This work was supported in part by 'Österreichische Nationalbank Jubiläumsfonds' through grant No 7694.

Notes added in proof. Recently, the critical properties of RIM were analyzed by means of a nonperturbative RG approach based on the concept of an effective average action [145]. The values of critical exponents obtained are in good agreement with the results of recent theoretical and experimental studies. Thus, the works [50, 145] remain the only theoretical studies where critical exponents were obtained by methods different from the field-theoretical RG approach.

[4] These numbers follow from the Fisher renormalization (11) applied to the pure ($d = 3$) Ising model exponents (4).

References

1. Stinchcombe R B, in *Phase Transitions and Critical Phenomena* Vol. 7 (Eds C Domb, J L Lebowitz) (New York: Academic Press, 1983) p. 151
2. Belanger D P *Braz. J. Phys.* **30** 682 (2000)
3. Parisi G, Ricci-Tersenghi F, Ruiz-Lorenzo J J *Phys. Rev. E* **60** 5198 (1999)
4. Dunlap R A, Gottlieb A M *Phys. Rev. B* **23** 6106 (1981)
5. Birgeneau R J et al. *Phys. Rev. B* **27** 6747 (1983)
6. Hastings J M, Corliss L M, Kunnmann W *Phys. Rev. B* **31** 2902 (1985)
7. Belanger D P, King A R, Jaccarino V *Phys. Rev. B* **34** 452 (1986)
8. Barrett P H *Phys. Rev. B* **34** 3513 (1986)
9. Mitchell P W et al. *Phys. Rev. B* **34** 4719 (1986)
10. Thurston T R et al. *Phys. Rev. B* **37** 9559 (1988)
11. Rosov N et al. *Phys. Rev. B* **37** 3265 (1988)
12. Belanger D P et al. *Phys. Rev. B* **37** 226 (1988)
13. Ramos C A, King A R, Jaccarino V *Phys. Rev. B* **37** 5483 (1988)
14. Ferreira I B, King A R, Jaccarino V *Phys. Rev. B* **43** 10797 (1991)
15. Belanger D P et al. *J. Magn. Magn. Mater.* **140 – 144** 1549 (1995)
16. Belanger D P et al. *Phys. Rev. B* **54** 3420 (1996)
17. Hill J P et al. *Phys. Rev. B* **55** 356 (1997)
18. Slanič Z, Belanger D P *J. Magn. Magn. Mater.* **186** 65 (1998)
19. Belanger D P, Slanič Z, Fernandez-Baca J A *J. Magn. Magn. Mater.* **177 – 181** 171 (1998)
20. Slanič Z, Belanger D P, Fernandez-Baca J A *Phys. Rev. Lett.* **82** 426 (1999)
21. Landau D P *Phys. Rev. B* **22** 2450 (1980)
22. Marro J, Labarta A, Tejada J *Phys. Rev. B* **34** 347 (1986)
23. Chowdhury D, Stauffer D *J. Stat. Phys.* **44** 203 (1986)
24. Braun P, Fähnle M *J. Stat. Phys.* **52** 775 (1988)
25. Braun P et al. *Int. J. Mod. Phys. B* **3** 1343 (1989)
26. Wang J-S, Chowdhury D *J. Phys.* (Paris) **50** 2905 (1989)
27. Wang J-S et al. *Physica A* **166** 173 (1990)
28. Holey T, Fähnle M *Phys. Rev. B* **41** 11709 (1990); Fähnle M, Holey T, Eckert J *J. Magn. Magn. Mater.* **104 – 107** 195 (1992)
29. Heuer H-O *Europhys. Lett.* **12** 551 (1990); Heuer H-O *Phys. Rev. B* **42** 6476 (1990)
30. Heuer H-O *J. Phys. A: Math. Gen.* **26** L333 (1993)
31. Prudnikov V V, Vakilov A N *Zh. Eksp. Teor. Fiz.* **103** 962 (1993) [*JETP* **76** 469 (1993)]
32. Hennecke M *Phys. Rev. B* **48** 6271 (1993)
33. Ballesteros H G et al. *Phys. Rev. B* **58** 2740 (1998)
34. Wiseman S, Domany E *Phys. Rev. Lett.* **81** 22 (1998)
35. Wiseman S, Domany E *Phys. Rev. E* **58** 2938 (1998)
36. Aharony A, Harris A B, Wiseman S *Phys. Rev. Lett.* **81** 252 (1998)
37. Marqués M I, Gonzalo J A *Physica A* **284** 187 (2000)
38. Marqués M I, Gonzalo J A *Phys. Rev. E* **60** 2394 (1999)
39. Marqués M I, Gonzalo J A, Íñiguez J *Phys. Rev. E* **62** 191 (2000)
40. Hukushima K *J. Phys. Soc. Jpn.* **69** 631 (2000)
41. Berche P E et al., in *MECO25, Middle European Cooperation in Statistical Physics, Pont-à-Mousson, France, 9 – 11 March, 2000*, p. 51; Berche P E et al. *Comput. Phys. Commun.* **147** 427 (2002)
42. Harris A B, Lubensky T C *Phys. Rev. Lett.* **33** 1540 (1974)
43. Khmel'nitskii D E *Zh. Eksp. Teor. Fiz.* **68** 1960 (1975) [*Sov. Phys. JETP* **41** 981 (1975)]
44. Lubensky T C *Phys. Rev. B* **11** 3573 (1975)
45. Grinstein G, Luther A *Phys. Rev. B* **13** 1329 (1976)
46. Jayaprakash C, Katz H J *Phys. Rev. B* **16** 3987 (1977)
47. Shalaev B N *Zh. Eksp. Teor. Fiz.* **73** 2301 (1977) [*Sov. Phys. JETP* **46** 1204 (1977)]
48. Sokolov A I *Fiz. Tverd. Tela* **19** 748 (1977) [*Sov. Phys. Solid State* **19** 433 (1977)]
49. Sokolov A I, Shalaev B N *Fiz. Tverd. Tela* **23** 2058 (1981) [*Sov. Phys. Solid State* **23** 1200 (1981)]
50. Newman K E, Riedel E K *Phys. Rev. B* **25** 264 (1982)
51. Jug G *Phys. Rev. B* **27** 609 (1983)
52. Mayer I O, Sokolov A I *Fiz. Tverd. Tela* **26** 3454 (1984) [*Sov. Phys. Solid State* **26** 2076 (1984)]
53. Shpot N A *Phys. Lett. A* **142** 474 (1989)
54. Mayer I O, Sokolov A I, Shalaev B N *Ferroelectrics* **95** 93 (1989)
55. Mayer I O *J. Phys. A: Math. Gen.* **22** 2815 (1989)
56. Holovatch Yu, Shpot M *J. Stat. Phys.* **66** 867 (1992)
57. Janssen H K, Oerding K, Sengespeick E *J. Phys. A: Math. Gen.* **28** 6073 (1995)
58. Shalaev B N, Antonenko S A, Sokolov A I *Phys. Lett. A* **230** 105 (1997)
59. Folk R, Holovatch Yu, Yavors'kii T *J. Phys. Stud.* **2** 213 (1998)
60. Holovatch Yu, Yavors'kii T *J. Stat. Phys.* **93** 785 (1998); *Condens. Mater. Phys.* (11) 87 (1997)
61. Folk R, Holovatch Yu, Yavors'kii T *Pis'ma Zh. Eksp. Teor. Fiz.* **69** 698 (1999) [*JETP Lett.* **69** 747 (1999)]
62. Varnashev K B *Phys. Rev. B* **61** 14660 (2000)
63. Folk R, Holovatch Yu, Yavors'kii T *Phys. Rev. B* **61** 15114 (2000)
64. Pakhnin D V, Sokolov A I *Pis'ma Zh. Eksp. Teor. Fiz.* **71** 600 (2000) [*JETP Lett.* **71** 412 (2000)]; *Phys. Rev. B* **61** 15130 (2000)
65. Pelissetto A, Vicari E *Phys. Rev. B* **62** 6393 (2000)
66. Carmona J M, Pelissetto A, Vicari E *Phys. Rev. B* **61** 15136 (2000)
67. Stanley H E *Introduction to Phase Transitions and Critical Phenomena* (Oxford: Clarendon Press, 1971)
68. Kouvel J S, Fisher M E *Phys. Rev.* **136** A1626 (1964)
69. Riedel E K, Wegner F J *Phys. Rev. B* **9** 294 (1974)
70. Wegner F J *Phys. Rev. B* **5** 4529 (1972)
71. Harris A B *J. Phys. C: Solid State Phys.* **7** 1671 (1974)
72. Chayes J T et al. *Phys. Rev. Lett.* **57** 2999 (1986)
73. Guida R, Zinn-Justin J *J. Phys. A: Math. Gen.* **31** 8103 (1998)
74. Emery V J *Phys. Rev. B* **11** 239 (1975); Edwards S F, Anderson P W *J. Phys. F: Met. Phys.* **5** 965 (1975)
75. Brout R *Phys. Rev.* **115** 824 (1959)
76. Fisher M E *Phys. Rev.* **176** 257 (1968)
77. Dotsenko V et al. *J. Phys. A: Math. Gen.* **28** 3093 (1995)
78. Dotsenko Vik S *J. Phys. A: Math. Gen.* **32** 2949 (1999)
79. Griffiths R B *Phys. Rev. Lett.* **23** 17 (1969)
80. Dotsenko V, Feldman D E *J. Phys. A: Math. Gen.* **28** 5183 (1995)
81. Wu X *Physica A* **251** 309 (1998)
82. Prudnikov V V, Prudnikov P V, Fedorenko A A *J. Phys. A: Math. Gen.* **34** L145 (2001)
83. Hutchings M T, Schulhof M P, Guggenheim H J *Phys. Rev. B* **5** 154 (1972)
84. Hutchings M T, Rainford B D, Guggenheim H J *J. Phys. C: Solid State Phys.* **3** 307 (1970)
85. Heller P *Phys. Rev.* **146** 403 (1966)
86. Dietrich O W *J. Phys. C: Solid State Phys.* **2** 2022 (1969)
87. Schullhof M P et al. *Phys. Rev. B* **1** 2304 (1969)
88. Wertheim G K, Buchanan D N E *Phys. Rev.* **161** 478 (1967)
89. Belanger D P, King A R, Jaccarino V *J. Appl. Phys.* **53** 2704 (1982)
90. Meyer G M, Dietrich O W *J. Phys. C: Solid State Phys.* **11** 1451 (1978)
91. Cowley R S, Carneiro K *J. Phys. C: Solid State Phys.* **13** 3281 (1980)
92. Belanger D P et al. *J. Magn. Magn. Mater.* **15 – 18** 807 (1980)
93. Gehring G A *J. Phys. C: Solid State Phys.* **10** 531 (1977)
94. Fishman S, Aharony A *J. Phys. C: Solid State Phys.* **12** L729 (1979)
95. Cardy J L *Phys. Rev. B* **29** 505 (1984)
96. Belanger D P, Young A P *J. Magn. Magn. Mater.* **100** 272 (1991)
97. Belanger D P, Lui M, Erwin R W, in *Magnetic Ultrathin Films: Symp., San Francisco, CA, USA, April 12 – 16, 1993* (Mater. Res. Soc. Symp. Proc., Vol. 313, Eds B T Jonker et al.) (Pittsburgh, Pa.: Materials Research Society, 1993) p. 755
98. Goldman A I et al. *Phys. Rev. B* **36** 5609 (1987)
99. Berche B, unpublished
100. Binder K (Ed.) *Monte Carlo Methods in Statistical Physics* (Topics in Current Physics, Vol. 7) (Berlin: Springer-Verlag, 1979)
101. Barber M N et al. *Phys. Rev. B* **32** 1720 (1985)
102. Swendsen R H, Wang J-S *Phys. Rev. Lett.* **58** 86 (1987); Wolff U *Phys. Lett. B* **228** 379 (1989)
103. Heuer H-O *Comput. Phys. Commun.* **59** 387 (1990)
104. Wiseman S, Domany E *Phys. Rev. E* **52** 3469 (1995)
105. Aharony A, Harris A B *Phys. Rev. Lett.* **77** 3700 (1996)
106. Weinrib A, Halperin B I *Phys. Rev. B* **27** 413 (1983)
107. Prudnikov V V, Fedorenko A A *J. Phys. A: Math. Gen.* **32** L399 (1999); Prudnikov V V, Prudnikov P V, Fedorenko A A *J. Phys. A: Math. Gen.* **32** 8587 (1999); *Phys. Rev. B* **62** 8777 (2000); Blavats'ka V, von Ferber C, Holovatch Yu *J. Mol. Liq.* **92** 77 (2001); *Phys. Rev. E* **64** 041102 (2001)

108. Brézin E, Le Guillou J C, Zinn-Justin J, in *Phase Transitions and Critical Phenomena* Vol. 6 (Eds C Domb, M S Green) (London: Academic Press, 1976); Amit D J *Field Theory, the Renormalization Group, and Critical Phenomena* 2nd ed. (Singapore: World Scientific, 1989)
109. Zinn-Justin J *Quantum Field Theory and Critical Phenomena* (Intern. Ser. of Monographs on Phys., 92) (Oxford: Clarendon Press, 1996); Kleinert H, Schulte-Frohlinde V *Critical Properties of ϕ^4-Theories* (River Edge, NJ: World Scientific, 2001); Pelissetto A, Vicari E *Phys. Rep.* **368** 549 (2002)
110. 't Hooft G, Veltman M *Nucl. Phys. B* **44** 189 (1972); 't Hooft G *Nucl. Phys. B* **61** 455 (1973)
111. Parisi G, in *Proc. of the Cargrése Summer School, 1973* (unpublished); Parisi G *J. Stat. Phys.* **23** 49 (1980)
112. Vladimirov V S *Uravneniya Matematicheskoĭ Fiziki* 3rd ed. (Equations of Mathematical Physics) (Moscow: Nauka, 1976) [Translated into English (Moscow: Mir, 1984)]
113. Nasser I, Folk R *Phys. Rev. B* **52** 15799 (1995)
114. Frey E, Schwabl F *Phys. Rev. B* **42** 8261 (1990)
115. Kleinert H, Schulte-Frohlinde V *Phys. Lett. B* **342** 284 (1995)
116. Nickel B G, Meiron D I, Baker G A "Compilation of 2pt and 4pt graphs for continuous spin model", Report (Ontario: University of Guelph, 1977)
117. Bervillier C, Shpot M *Phys. Rev. B* **46** 955 (1992)
118. Mayer I *Physica A* **252** 450 (1998)
119. Holovatch Yu, Krokhmal's'kii T *J. Math. Phys.* **35** 3866 (1994)
120. Wilson K G, Fisher M E *Phys. Rev. Lett.* **28** 240 (1972)
121. Schloms R, Dohm V *Europhys. Lett.* **3** 413 (1987); *Nucl. Phys. B* **328** 639 (1989)
122. Le Guillou J C, Zinn-Justin J *Phys. Rev. B* **21** 3976 (1980)
123. Newlove S A *J. Phys. C: Solid State Phys.* **16** L423 (1983)
124. Shpot N A *Zh. Eksp. Teor. Fiz.* **98** 1762 (1990) [*Sov. Phys. JETP* **71** 989 (1990)]
125. von Ferber C, Holovatch Yu *Europhys. Lett.* **39** 31 (1997); *Phys. Rev. E* **56** 6370 (1997); **59** 6914 (1999); Folk R, Holovatch Yu, Yavors'kii T *Phys. Rev. B* **62** 12195 (2000)
126. Folk R, Holovatch Yu, in *Correlations, Coherence, and Order* (Eds D V Shopova, D I Uzunov) (New York: Kluwer Acad./Plenum Publ., 1999) p. 83
127. Hardy G H *Divergent Series* (Oxford: Clarendon Press, 1949)
128. Eckmann J-P, Magnen J, Seneor R *Commun. Math. Phys.* **39** 251 (1975)
129. Lipatov L N *Zh. Eksp. Teor. Fiz.* **72** 411 (1977) [*Sov. Phys. JETP* **45** 216 (1977)]
130. Brézin E, Le Guillou J C, Zinn-Justin J *Phys. Rev. D* **15** 1544 (1977)
131. Brézin E, Parisi G *J. Stat. Phys.* **19** 269 (1978)
132. Bray A J et al. *Phys. Rev. B* **36** 2212 (1987)
133. McKane A J *Phys. Rev. B* **49** 12003 (1994)
134. Baker G A (Jr) et al. *Phys. Rev. Lett.* **36** 1351 (1976); Baker G A (Jr), Nickel B G, Meiron D I *Phys. Rev. B* **17** 1365 (1978)
135. Álvarez G, Martín-Mayor V, Ruiz-Lorenzo J J *J. Phys. A: Math. Gen.* **33** 841 (2000)
136. Baker G A (Jr), Graves-Morris P *Padé Approximants* (Reading, MA: Addison-Wesley, 1981)
137. Watson P J S *J. Phys. A: Math. Gen.* **7** L167 (1974)
138. Chisholm J S R *Math. Comp.* **27** 841 (1973)
139. Folk R, Holovatch Yu, Yavors'kii T, unpublished
140. Zinn-Justin J *Phys. Rep.* **70** 109 (1981)
141. Holovatch Yu *Lectures on Critical Phenomena: Polymers, Diluted Systems, Magnets* (Linz, 1996) (unpublished)
142. Pitard E et al. *Phys. Rev. Lett.* **74** 4361 (1995)
143. Yoon J, Chan M H W *Phys. Rev. Lett.* **78** 4801 (1997); Zassenhaus G M, Reppy J D *Phys. Rev. Lett.* **83** 4800 (1999)
144. Lipa J A et al. *Phys. Rev. Lett.* **84** 4894 (2000)
145. Tissier M T et al. *Phys. Rev. B* **65** 140402(R) (2002)